An Efficient Drive, Sensing, and Actuation System using PZT Stack Actuator Cells

by

Patrick R. Barragán

B.S., Mechanical Engineering, Massachusetts Institute of Technology, 2008

and

B.S., Electrical Engineering and Computer Science, Massachusetts Institute of Technology, 2008

Submitted to the Department of Mechanical Engineering and the Department of Electrical Engineering and Computer Science in partial fulfillment of the requirements for the degrees of

Master of Science in Mechanical Engineering

and

Master of Science in Electrical Engineering and Computer Science

at the

MASSACHUSETTS INSTITUTE OF TECHNOLOGY

February 2012

Author ..
Department of Mechanical Engineering and Department of Electrical Engineering and Computer Science
July 13, 2011

Certified by .....
H. Harry Asada
Ford Professor of Mechanical Engineering
Thesis Supervisor

Accepted by ....
David E. Hardt
Chairman, Department Committee on Graduate Students
Department of Mechanical Engineering

Accepted by ...
Leslie A. Kolodziejski
Chairman, Department Committee on Graduate Students
Department of Electrical Engineering and Computer Science

An Efficient Drive, Sensing, and Actuation System using PZT Stack Actuator Cells

by

Patrick R. Barragán

Submitted to the Department of Mechanical Engineering and the Department of Electrical Engineering and Computer Science
on July 13, 2011, in partial fulfillment of the
requirements for the degrees of
Master of Science in Mechanical Engineering
and
Master of Science in Electrical Engineering and Computer Science

Abstract

The PZT cellular actuator developed in the MIT d'Arbeloff Laboratory utilizes small-strain, high-force PZT stack actuators in a mechanical flexure system to produce a larger-strain, lower-force actuator useful in robotic systems. Many functionalities for these cellular actuators are developed which can have great impact on robotic systems and actuation itself. After initial exploration into other possible circuitry, a circuit is designed to recovery unused energy for the PZT cells. The circuit design is formed around a proposed method of distributed actuation using PZT cells which imposes that different PZT cells will be activated during different periods such that the charge from some cells can be transferred to others. If the application allows actuation which can conform to this criteria, the developed circuit can be used which, without optimization, can save ~41% of the energy used to drive the actuators with a theoretical upper limit on energy efficiency of 100%. A dynamic system consisting of multiple PZT actuators driving a linear gear is analyzed and simulated which can achieve a no load speed 2.4 $[\frac{m}{s}]$ with minimal actuators. Then, the two-way transforming properties of PZT stack actuators are utilized to allow dual sensing and actuation. This method uses an inactive PZT cell as a sensor. With no additional sensors, a pendulum system driven by antagonistic groups of PZT cells is shown to find its own resonance with no system model. These functionalities of charge recovery, distributed actuation, and dual sensing and actuation set the PZT cellular actuator as an important contribution to robotic actuation and begin to illuminate the possible impacts of the concept. The design and analysis described reveals many possibilities for future applications and developments using the PZT cellular actuator in the fields of actuation and robotics.

Thesis Supervisor: H. Harry Asada
Title: Ford Professor of Mechanical Engineering

Acknowledgments

First, I would like to thank the Lord Jesus without whom nothing is possible. Second, I would like to thank my family for sacrificing so much to give me the opportunities I have today. I would like to thank my father's parents Mauricio and Rebecca Barragán and my mother's parents Florentino and Zoraida Couce. Without their tireless work and love, my family would not have survived in this country. I would like to thank my parents Blas Sr. and Maria. Without their never ending sacrifices, I would never have the opportunities that I have today. I would like to thank my brother Blas Jr. He taught me how to think and analyze and kept me on a straight path. I owe him dearly. I would like to thank my grandmother Zoraida in a special way for helping raise me while my parents had to work. Without her sacrifices for me and the rest of my family, we would have no chance at anything we have managed or ever will manage. A person is nothing without their family. Yo no puedo ser nada sin mi familia.

I would also like to thank my advisor Professor H. Harry Asada for his help in this project and guidance in research in general. Also, I give great thanks to the past and present members of the d'Arbeloff laboratory for all of their help. Next, I would like to specially thank my friend Victor Sinow for the hours and hours he spent helping me despite having no connection to the project or lab and getting nothing in return. He has shown what true friendship is. Finally, I would like to thank all of my friends for helping me every step of the journey. I could not have survived without you.

And finally, to Dave Wottle, I made it again.

Contents

List of Figures

Chapter 1

Introduction

1.1 Original Intention

Research has sought to develop novel actuators for robotic applications. Electric motors, solenoids, and hydraulics have been used extensively in robotics but may be mismatched for certain applications. Many types of smart materials including shape memory alloy, piezoelectric materials, and others have been used in this research goal [1, 2].

Lead zirconate titanate (PZT) is a type of piezoelectric material which converts energy both ways between the electrical and mechanical domains. Electrical charge can be driven onto the PZT to create small mechanical deformations. Conversely, mechanical force can be applied to the PZT to produce an electrical voltage. Because only a fraction of the electrical energy driven to a PZT is converted to mechanical work and PZT is electrically capacitive in nature, an opportunity exists to use the energy remaining on the PZT after actuation [3]. This work aims to explore possible circuitry to take advantage of this unused energy and increase the electrical efficiency of driving PZT actuators.

Additionally, past and concurrent research has sought to amplify the output displacement of PZT to a level usable for standard robotic applications at the cost of reducing the PZT's very substantial output force. The mechanical amplification techniques utilize multiple PZT stack actuators, which consist of many layers of PZT

material, in flexure systems or special configurations creating PZT cells [2].

Initially, the desired functionality of the circuit was to charge the PZT cells to a necessary voltage, recover charge back to a battery when the cells must be deactivated, and harvest energy from external mechanical stimulus. This functionality could be created by three separate circuits to achieve each part. However, complexity, weight, and power consumption made a single circuit with all functionality desirable if such a circuit could outperform the separated circuits in these metrics.

A bidirectional flyback converter could achieve all three functionalities. This converter was designed, implemented, and tested. The results suggested that this type of active circuit may be somewhat mismatched with the low power necessary for the PZT cells. The low power that could be harvested from mechanical stimulus also made the harvesting goal impractical for systems on the scale tested and thus was abandoned.

1.2 Shifted Goals

Instead, a new option to create an efficient power circuit for the PZT cells was chosen. Because of the extremely low power of driving a single PZT cell, care had to be taken to reduce energy transfer steps and resistance in the transfer path. Driving energy back to a storage medium or battery first and then back to the PZT cells became undesirable assuming some inefficiency in each transfer. Instead, a circuit was developed to transfer energy between sets of PZT cells directly. Without optimization, the designed circuit could save $\sim$41% of the energy used to drive the actuators with a theoretical limit of 100%. A distributed actuation scheme was then developed to take advantage of this type of PZT cell to PZT cell transfer while properly actuating a load. An example is considered in detail to demonstrate the possibilities of this scheme.

1.3 New Opportunities

Because of the actuation drive scheme, sets of PZT cells are left uncharged after transferring their energy to newly actuating sets. Allowing the discharged PZTs to float electrically allows these PZT cells to be utilized as sensors. In this manner, the same PZT cell can be used interchangeably as an actuator and a sensor. These dual functionalities were utilized for resonance determination in which the same sets of PZTs oscillate a load and concurrently determine the system resonance using an initial frequency sweep. An example system demonstrates this functionality. Resonance determination is only one of the possible applications of the cells' dual sensing and actuation capability.

The PZT drive system developed considers efficiency when creating a practical actuation scheme. Because of the cell to cell transfer architecture chosen, significant energy can be saved, and additional functionalities such as the dual sensing and actuation scheme above can be applied.

Chapter 2

Charging, Recovery, and Actuation Scheme

2.1 Overall Approach

The original intention of the drive circuitry for the PZT cells hoped to achieve the three functionalities of charging, recovery, and actuation. First, the circuit should be able to drive the PZT cell to at least 150 [V] from a battery. Second, the circuit should be able to pull the energy back (recover) from the PZT cell to the battery or other storage medium. Third, the circuit should be able to pull (harvest)energy generated by external mechanical stimulus back to a battery or other storage medium from the PZT cell. After exploring these functionalities using an active circuit described below, low PZT cell power concerns and problems caused a shift in the desired functionality of the circuit. The new aim is described in 3. Below, the development, tests, and drawn conclusions are discussed for the original functionality.

2.2 Bi-directional Flyback Converter Topology

2.2.1 Transformer Model

An ideal transformer is modeled as shown in 2-1. The transformer is modeled as two coupled inductors. The two parallel lines in between represent the inductors' coupled nature. The left inductor with index 1 is referred to as the primary side and has an inductance L_1 in Henries. The right inductor with the index 2 is the secondary side and has an inductance L_2 in Henries. The transformer turns ratio is shown as N_1:N_2 indicating that the ratio of turns on the primary side to the turns on the secondary side is N_1/N_2.

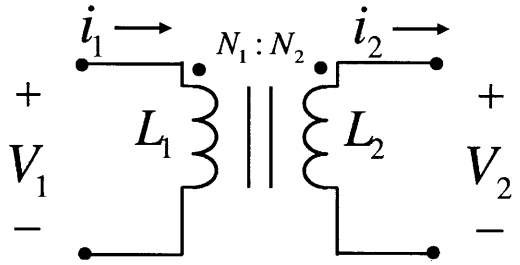

Figure 2-1: Ideal transformer model.

The voltages and currents in the transformer are also related by the turns ratio. The relationships are as follows:

$$\frac{V_1}{N_1} = \frac{V_2}{N_2}$$
$$i_1 N_1 = i_2 N_2$$

Thus, the ratio of the voltages is directly proportional to the turns ratio while the ratio of the currents is inversely proportional to the turns ratio.

The dot convention for transformers is important to understanding the direction of the currents in the transformer and the polarity of the voltages on the primary and secondary sides. The placement of the dots will indicate these parameters in a circuit diagram. This discussion assumes power flows from left to right in the diagram. However, the same reasoning applies for power flowing from right to left. Consistent with 2-1, the dots next to each inductor in the transformer will be placed where the

positive voltage will be induced on that side of the transformer. A positive V_1 will induce a positive V_2 where the positive polarity is on the side of the inductor indicated by the dot. Additionally, an ideal transformer is 100% efficient. Power in will be equal to power out. Thus, with a positive voltage on the primary side inductance, positive current will flow into the dot on the primary side. With a positive voltage on the secondary side (which will be induced by the positive voltage on the primary side), current will flow out of the dot on the secondary side. Again, by the same arguments, if power flows from right to left in the diagram, only the direction of the both currents i_1 and i_2 will flip.

Real transformers have many parasitics which are not captured in the ideal model. One important parasitic is the magnetizing inductance. The magnetizing inductance models the magnetization of the core material of the transformer as current flows through the windings. The magnetizing inductor is modeled as a separate inductor from the primary and secondary winding inductors. This inductance, often designated as L_μ, is placed in parallel with the primary or secondary side inductor in the model. With the standard placement, 2-2 shows the model of the transformer including the magnetizing inductance in parallel with the primary side inductor. If L_μ was reflected to appear on the secondary side, L_μ would be in parallel with L_2 and have a value $L_\mu(N_2/N_1)^2$.

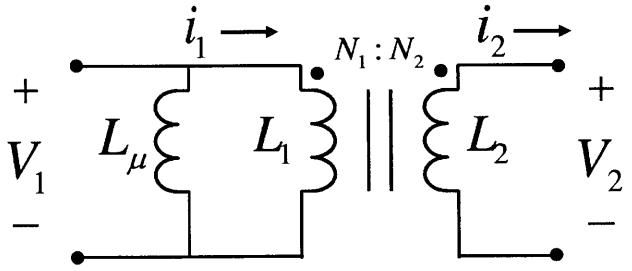

Figure 2-2: Transformer model with the parasitic magnetizing inductance on the primary side.

The difference in definition of i_1 is important to note. The current i_1 is not defined as the current into the input terminal of the transformer but rather the current into the primary side inductor L_1. This difference means that some amount of the current flowing into the input terminal of the transformer will flow through the magnetizing

inductance with the remainder as i_1. Transformers involve many other parasitics which are important for various applications. The application and its parameters will indicate which parasitics must be accounted for and which can be ignored.

2.2.2 Flyback Converter

The flyback converter is a DC to DC power converter topology. This particular topology utilizes the magnetizing inductance parasitic of its transformer for its function. Without the magnetizing inductance, the converter would not work. In general, the transformer for this converter is designed with an air gap in its core in order to increase the magnetizing inductance as much as possible for its size. In this way, the magnetizing inductor can store the most energy for its size.

2-3 shows the flyback converter topology. Power flows from left to right in this converter. A power source V_{in} provides the energy which will eventually be transmitted to load impedance Z_L to generate the output voltage V_{out}. C_i and C_o act as the input and output filter capacitors respectively which smooth out variations in their corresponding input and output voltages. A switch S_1 is an active element in the circuit driven externally. This switch generally operates on a repeating switching cycle with some fraction of the cycle with the switch closed and some fraction of the cycle with the switch open. The ratio of time with a closed switch to time with an open switch is referred to as the duty ratio of the cycle. Both the period of the switching cycle and the duty ratio of the switch may be fixed or variable.

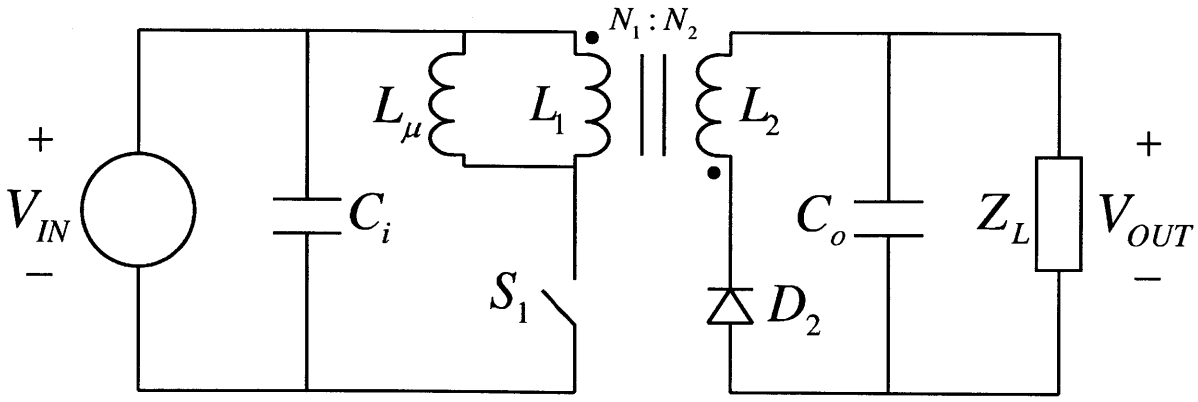

Figure 2-3: Flyback converter topology.

In the first part of each cycle, S_1 closes. When the switch is closed, the voltage V_{in} is across the primary side of the transformer. A positive voltage V_{in} would cause current to flow through the L_μ and L_1. However, because current could flow into the dot on L_1 and thus have to flow out of the dot on L_2, no current flows through L_1 because diode D_2 prevents this flow. Thus, L_μ is charged. When S_1 opens during the second part of the cycle, the magnetizing inductance attempts to keep current flowing through it in the same direction. The only outlet for this flow is to drive current through the loop made by L_μ and L_1. Current flows out of the dot on L_1 and thus into the dot on L_2. Diode D_2 now allows this current to pass. The current then flows and splits in some proportion between the output capacitor and Z_L. In this manner, V_{in} transfers a packet of energy to the output impedance every cycle.

Using periodic steady state (PSS) analysis, an input voltage to output voltage relationship can be found. PSS assumes that the converter has reached a steady ripple oscillation with all voltages and currents. In PSS, the average current through capacitors and average voltage across inductors must be equal to zero over a cycle. These constraints come directly from the definition of PSS. Let D be the duty ratio of S_1. D can vary between 0 and 1. Then, the average voltage across the magnetizing inductance is given by:

$$< V_{L_\mu} >= DV_{IN} + (1 - D)\frac{N_1}{N_2}(-V_{OUT}) = 0$$

Rearranging this equation for a voltage in to voltage out relationship yields:

$$V_{OUT} = \frac{N_2}{N_1}\frac{D}{1 - D}V_{IN}$$

V_{out} depends on the turns ratio of the transformer, the duty ratio, and the input voltage. As D varies from 0 to 1, the gain, $(N_2/N_1)(D/(1-D))$, in front of V_{in} in the above equation goes from 0 to infinity. Therefore, the flyback converter can produce output voltages higher and lower than the input voltage.

2.2.3 Bidirectional Flyback Converter

The bidirectional flyback converter is extremely similar to the flyback converter except the bidirectional topology allows power to flow from left to right and from right to left. Shown in 2-4, this functionality is achieved by adding a primary side diode in parallel with S_1 and a secondary side switch in parallel with D_2.

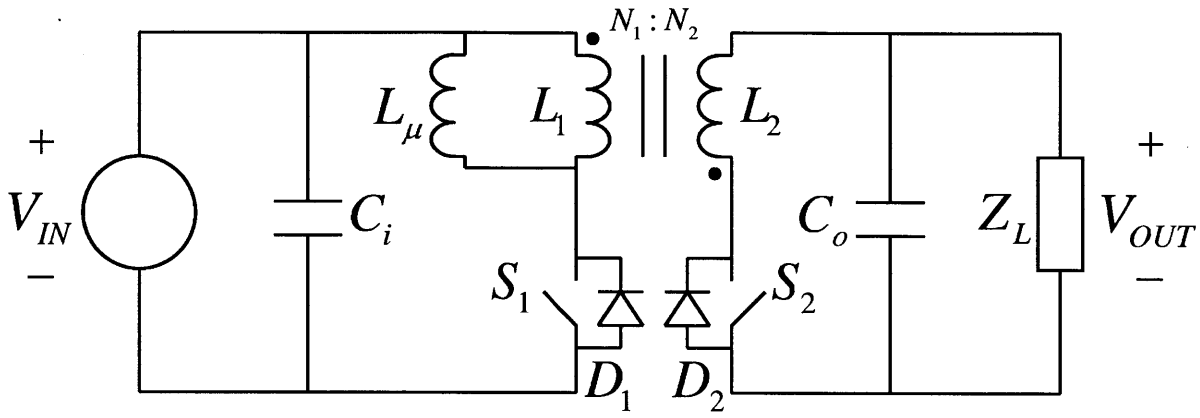

Figure 2-4: Bidirectional flyback converter topology.

The forward direction of operation (power flowing from left to right) works exactly the same as discussed above for the flyback converter. The diode D_1 does not affect the operation of this mode because in this mode, current is never drawn in the direction D_1 can allow. Also, S_2 is always left open in forward operation. Therefore, when operating in the forward direction, the converter works in the same manner as it would with D_1 and S_2 removed.

The backward direction of operation (power flowing from right to left) operates as a mirror of the forward direction. Because L_μ can be reflected to the secondary side, the circuit diagram can be flipped and redrawn to look essentially identical to 2-4. 2-5 shows this mirrored converter:

As discussed above, the value $L_{\mu 2}$ of the magnetizing inductance reflected to the secondary side would be $L_\mu(N_2/N_1)^2$. The flipped dots on the transformer may appear at first to indicate some difference in operation. However, that the dots are opposite each other in both 2-4 and 2-5 indicates that the operation of the transformer in the circuit has not changed.

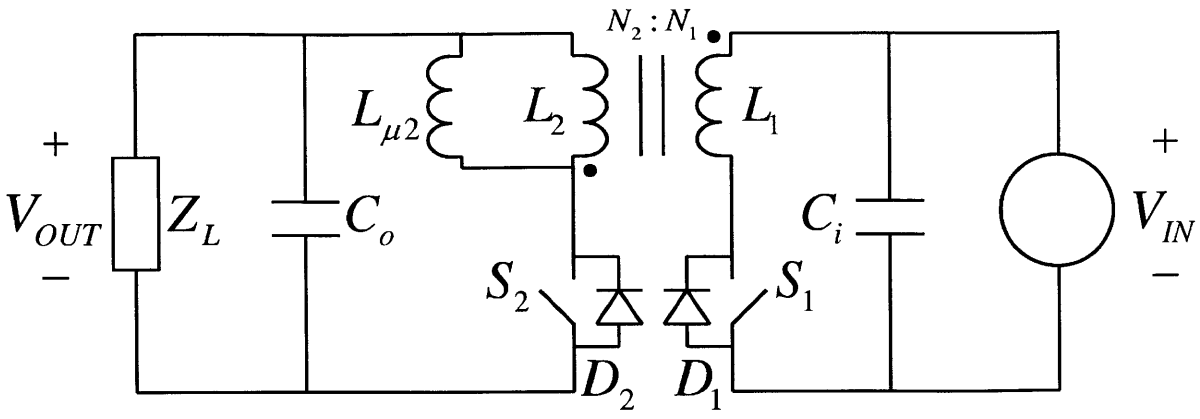

Figure 2-5: Mirrored version of the bidirectional flyback converter topology.

Comparing 2-4 and 2-5 clearly indicates the essentially identical operation. In the backward direction, the converter uses S_2 and D_1 to transfer packets of energy from the output V_{out} to the input V_{in}. Because of the same arguments as above for the forward direction, the backward direction of operation functions in the same manner as it would with D_2 and S_1 removed. Thus, the backward direction of operation also works off of the same principles of operation as discussed for the flyback converter. The bidirectional flyback converter can transfer packets of energy from input to output and back.

2.3 Charge Recovery and Energy Harvesting

2.3.1 PZT Stack Model

The ideas of charge recovery and energy harvesting using PZT stack actuators are closely related. PZT stack actuators are two-way electromechanical transformers. This ability allows the stacks to convert electrical power into mechanical power and the reverse. The simplest electrical model of a PZT stack actuator is a capacitor. When the actuator is activated (the actuator extends), the voltage applied across the actuator must charge this capacitor. Conversely, when the actuator is deactivated (the actuator contracts), the charge on this capacitor must be removed. On the mechanical side, when the actuator is mechanically compressed, charge is built up on

this capacitor. When the actuator is allowed to return to its resting configuration, the charge must dissipate.

These ideas can be clearly expressed in a bond graph model of the PZT stack actuator. A bond graph is a diagram which shows energy flow between different components of a dynamic system. 2-6 shows the most basic bond graph model of the PZT stack actuator.

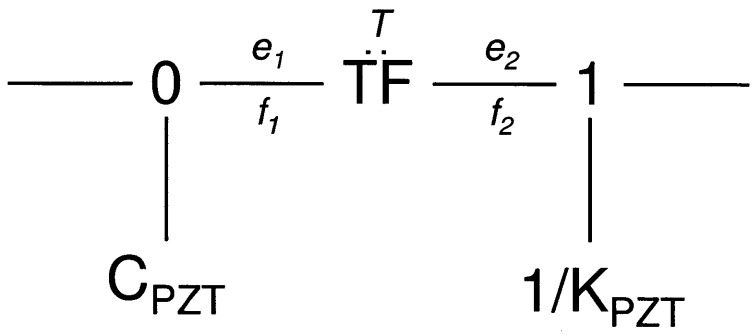

Figure 2-6: Basic, idealized bond graph model of the PZT stack actuator.

Each line shows a path on which energy can flow. Associated with each line are a flow variable and an effort variable with power as the product of the two. The 0 and 1 in the diagram represent two different types of junctions where multiple energy flows meet. The value of each effort variable meeting at a 0 junction is the same. The flow variables sum at a 0 junction. The 1 junction is the opposite with the effort variables summing and the value of the flow variables being equal. At each junction, power must be conserved. Therefore, the power going into the junction is equal to power leaving such that no power is stored at the junction.

Three additional elements appear in this bond graph model. The stack's electrical capacitance is represented as C_{PZT} and is connected to the 0 junction. The stack's mechanical stiffness is represented as K_{PZT}. By using the inverse of this stiffness $1/K_{PZT}$, also known as the compliance, the element becomes dimensionally equivalent to the electrical capacitance and appropriate for use in the energy flow model. The mechanical compliance is connected to the 1 junction. The final additional element is the two-way transformer represented as TF with a scaling ratio T. The transformer in the bond graph converts energy between the electrical and mechanical domains. In

the bond graph, the transformer is perfectly efficient. No power is lost in conversion between domains. The power on each side of the transformer is the product of the values of the flow and effort variables. Thus, the T scaling factor refers to amplifying one of these variables while attenuating the other in the new domain. 2-6 shows the effort and flow variables associated with the two bonds connected to the transformer. For a transformer represented in this way, the variables are scaled as follows:

$$e_1 = Te_2$$
$$f_2 = Tf_1$$

Multiplying the appropriate variables together verifies that power is conserved through the transformer:

$$P_1 = e_1 f_1 = Te_2 \frac{1}{T} f_2 = e_2 f_2 = P_2$$

The transformer relates one effort variable to the other and one flow variable to the other. Although the variables do not need to take the same value in the different domains, they must be scaled such that power is conserved as shown above. The placement of the capacitances in the bond graph suggests that the electrical domain is on the left of the transformer in 2-6 while the mechanical domain is on the right.

Other important elements of bond graphs are sources and sinks. Sources and sinks are known as active elements because the supply (or remove) energy from the system indefinitely. Therefore, sources and sinks change the system energy in the same way regardless of system parameters. These two elements can be of the effort or flow type. For example, an ideal voltage source could be considered an effort source in the electrical domain. In this domain, voltage is an effort variable indicating that an ideal voltage source is considered an effort source.

An ideal voltage source used to drive the PZT stack actuator would be represented as a source of effort, S_e, as shown in 2-7 below.

The source of effort adds power to the system through the bond between itself and the 0 junction. Some portion of this power goes to charging the PZT capacitance

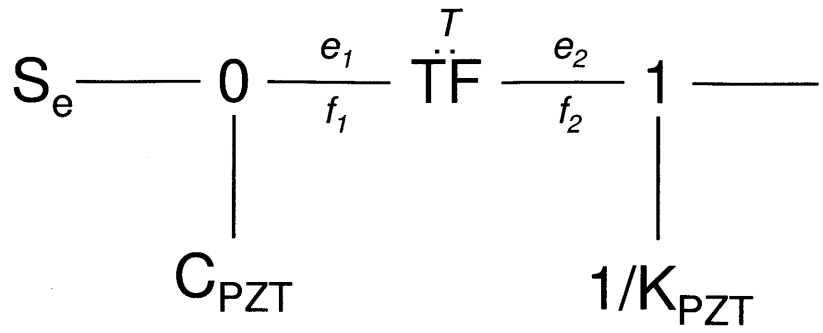

Figure 2-7: Simple bond graph model of the PZT stack actuator with an electrical effort source.

C_{PZT}. The remainder travels through the transformer into the mechanical domain. Some portion of this power in the mechanical domain goes to displace the stack's compliance $1/K_{PZT}$. Where the remaining power goes is currently undetermined. The right most bond in 2-7 does not have a specified element attached to one side. This currently empty node may be another junction to a bond graph representing the system that the PZT interacts with or may be a single element such as a mass that the PZT drives in the mechanical domain.

This system setup is only one of many possible setups for the PZT. For example, instead of being electrically driven, the stack actuator could be mechanically stimulated. An effort source could be placed on the right side of the bond graph in 2-6. The force source would provide power to system. As in the previous reasoning, some portion of the provided power would be transmitted to the leftmost bond. This bond could be connected to a single element, another bond graph model of an interacting system, or nothing. The system which interacts electrically with the PZT stack would determine the exact power flows in the bond graph model.

2.3.2 Basic Architecture

The ideas of charge recovery and energy harvesting are related to this removal or dissipation of charge on the actuator when the actuator returns from a charged state to a discharged state. The basic scheme for charge recovery is illustrated in 2-8 below. The PZT stack actuator is charged with a battery causing the actuator to expand.

When the actuator should contract, the energy built up on the actuator capacitance is driven back to the battery instead of merely dissipated through some resistance. By recovering some portion of the charge from the actuator every activation and deactivation cycle, the battery source will have an extended lifetime.

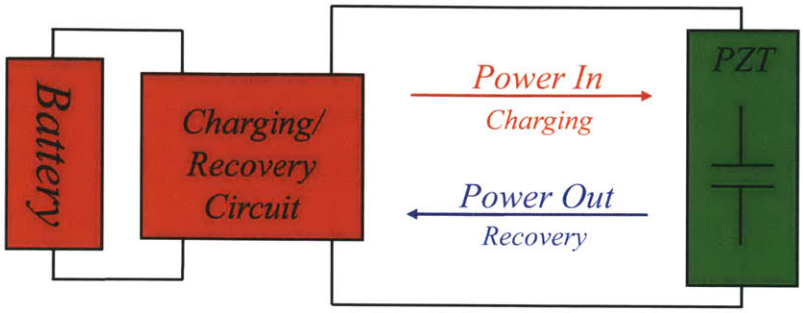

Figure 2-8: Basic charge recovery scheme.

Similarly, energy harvesting removes charge built up on the PZT stack actuator and drives it to the battery. The basic scheme of energy harvesting is illustrated in 2-9 below. A mechanical stimulus causes compression of the actuator. This compression builds up charge on the stack capacitance. This energy is driven from the actuator to the battery. If this mechanical stimulus is oscillatory in nature, harvested energy from each cycle of the stimulus can be used to recharge the battery. A newly recharged battery could then be used to power the actuator for subsequent activation and deactivation cycles.

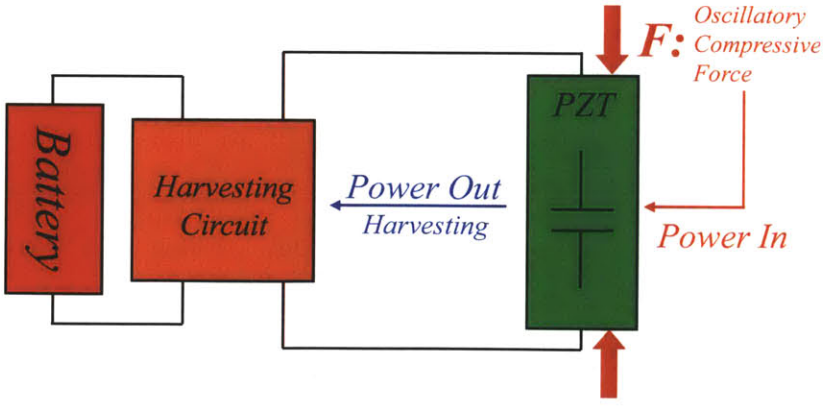

Figure 2-9: Basic energy harvesting scheme.

While one recovers unused energy and one transforms mechanical power into elec-

trical power, both schemes aim to increase the system's battery life. With increased battery life, a robotic system utilizing the PZT stack actuator could carry out a given task longer. With charge recovery, regular activation and deactivation cycles for the actuator require less energy allowing the actuator to run for longer on a given battery. With energy harvesting, a discharged or slightly discharged battery can be recharged to allow the actuator to carry out additional cycles not available with only the battery's initial power. Also, energy harvesting could provide the robotic system with a means of carrying out certain tasks (such as low power wireless communication) with no initial charge in the battery. In this way, certain tasks could still be available to the system (such as a distress call, etc.) even after the system has no internal power available.

Another closely related purpose for this functionality is to decrease the needed battery size for a given task. This function follows exactly from the previous desire to increase the battery life of the battery in a PZT actuator system. Increasing battery life is essentially equivalent to increasing efficiency for a given cycle or task. With the assumption that battery energy scales proportionally with battery weight, increasing this efficiency leads to less required battery energy for some given set of tasks and therefore, less battery and overall system weight for these actuator systems. This reduction of weight for the same usage time or amount proves crucial for mobile robotic applications. For example, a robotic fish utilizing PZT stack actuators for propulsion would have to propel its own weight through the water. With reduced weight, this task would be easier for the actuators. Therefore, harvesting energy and recovering charge to reduce the necessary battery size reduces the system weight which allows the system to save even more energy by not having to move the additional mass of more batteries.

2.4 Use of Bi-directional Flyback Converter for Charge Recovery and Energy Harvesting

The bi-directional flyback converter is one possible topology that would allow charge recovery and energy harvesting from a PZT stack actuator. 2-10 below shows the converter with the PZT placed as the load impedance.

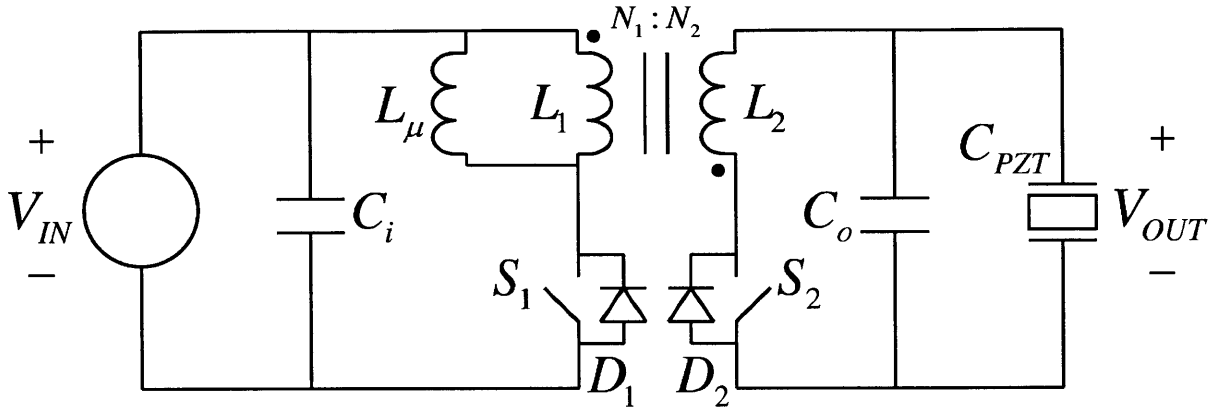

Figure 2-10: Bidirectional flyback converter driving a PZT stack actuator as the load.

The PZT stack's capacitive electrical model is a simplification which ignores the stack's coupling to the mechanical domain. For charging, charge recovery, and energy harvesting to occur, the input energy source must have the ability to source, sink, and store energy.

The bi-directional nature of the converter allows for both charge recovery and energy harvesting. As described previously, the converter works in the forward direction (power flowing from left to right) in order to charge the PZT stack. The packets of energy sent to the output by the converter each cycle charges the PZT's capacitance which causes the PZT stack to elongate. In order to deactivate or shorten the stack, the charge must be removed from this capacitance. As discussed previously, the charge could be dissipated through some resistance by grounding the PZT. However, to avoid wasting the built up energy on the PZT, the converter running in the backward direction drives the charge away from the output back to the input shown as V_{in} in 2-10. In this way, the charge is recovered to the input energy source and the PZT stack is deactivated. Saving this charge allows a finite input energy source

to power the PZT stack for more activation-deactivation cycles.

Energy harvesting also occurs with backward operation of the converter. For the converter to harvest energy, the PZT stack must be mechanically stimulated. Upon compression, the PZT stack will have charge built up on its capacitance. While the PZT has built up charge, the converter operating in the backward direction can drive the PZT's charge to the input energy source. With sufficient compression and harvesting cycles, the input energy source could be recharged. If this energy source also sources energy for other circuits, the harvested energy could be used to drive those circuits as well as reactive the PZT stack when necessary. In this way, even if at some point insufficient power is generated from harvesting to drive the PZT stacks, other lower power circuits such as wireless communicators or low-power displays could be powered only by the energy harvested from the mechanical environment.

Because only a finite amount of energy can be harvested from compression of a PZT stack, constant power flow from harvesting would require a cyclic mechanical stimulus. The frequency and amplitude of the mechanical stimulus would dictate the maximum possible power to be harvested. Some possible mechanical stimuli include ambient vibrations, compression due to footfall, and unsteady fluid flows.

2.5 Converter Implementation

2.5.1 Choosing Parameters

Magnetizing Inductance

The value of the magnetizing inductance L_μ is important for the proper function of the converter. The purpose of this inductance is to deliver packets of energy from one side of the converter to the other. During the first part of each switch cycle current ramps up in the inductor to same value I_{pk} and then ramps down during the second part.

Choosing this inductance value requires a desired amount of energy to be transferred in the converter per cycle. With perfect efficiency, the converter will transfer

a packet of energy per cycle as follows:

$$E_{cyc} = \frac{1}{2} L_\mu I_{pk}^2$$

This equation comes directly from the current signal curve with respect to time. Thus, increasing I_{pk} has the greatest effect on the energy per cycle. Driving the PZT stack through a change of voltage ΔV requires a transfer of energy equal to:

$$E_{\Delta V} = \frac{1}{2} C_{PZT} (\Delta V)^2$$

Therefore, from these equations, the number of cycles n required for causing this voltage change becomes:

$$n = \frac{C_{PZT} (\Delta V)^2}{L_\mu I_{pk}^2}$$

Minimizing the number of cycles required for a voltage change on the stack would minimize the time for charging and thus increase the speed of response of the system. The above equation shows that increasing I_{pk} has the greatest effect on decreasing n for a given ΔV. However, the magnetizing inductance is physically linked to the transformer used. The physical transformer suffers from two realities that limit the value of I_{pk}. First, magnetic flux B circulates through the core of the transformer. This flux is linked to the current flowing through the coils through physical parameters of the core material. As the current in the coils increases, the magnetic flux through the core increases. However, at some value B_{sat}, the core saturates. Thus, I_{pk} cannot be increased indefinitely without causing saturation of the core. Second, the coils of the transformer are constructed from wire wound around the core. As with any wire, increasing the current through the wire causes the wire to heat up due to resistive losses. At some point, this heat destroys the wire. I_{pk} cannot be increased indefinitely without causing heating problems in the transformer. In general, increasing the size of the transformer can increase the B_{sat} value for the core and can increase the wire diameter of the coils allowing the transformer to support a larger peak current. However, the transformer tends to dominate the mass of the circuit in these converters.

Increasing the size of the transformer also increases the weight. This increase in weight is very apparent in the total weight of the circuit. Because the circuitry is meant for mobile robotic applications, the total weight must be considered carefully. The purpose of the circuitry is to not only drive the PZT stacks but also save or harvest energy and thus save battery weight with an end goal to decrease overall system weight. If the required circuitry adds more mass to the system than it decreases with saved battery weight, the purpose of the circuit is lost. Therefore, the overall circuit weight, which is dominated by the mass of the transformer, is an essential consideration in the design of the system. In essence, the design must trade off speed of system response with circuit weight.

Switch Implementation

The converter utilizes two active switches, S_1 and S_2, and two passive switches, D_1 and D_2, in its operation. The pairs of switches S_1 and D_1 and S_2 and D_2 can be implemented using only two physical MOS field effect transistor (MOSFET) switches. As shown in 2-11, a MOSFET can implement the functionality of both the switch and the diode.

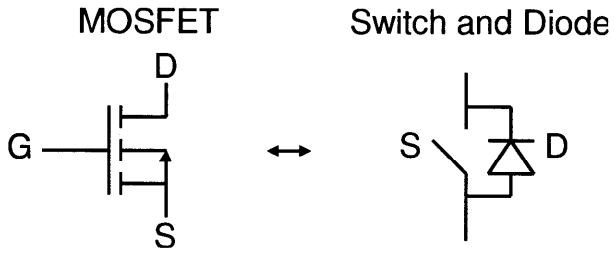

Figure 2-11: The use of a MOSFET implements both the ideal switch and diode functionalities.

Because of the placement of particular sections of doped silicon, the MOSFET achieves both functionalities. This MOSFET diode is referred to as its body diode. In the original converter diagram, no path for control of the circuits was shown. Replacing the switch and diode with the MOSFETs is shown in 2-12.

The circuit functionality is controlled through the gates of the two MOSFETs, labeled G, by an outside control source.

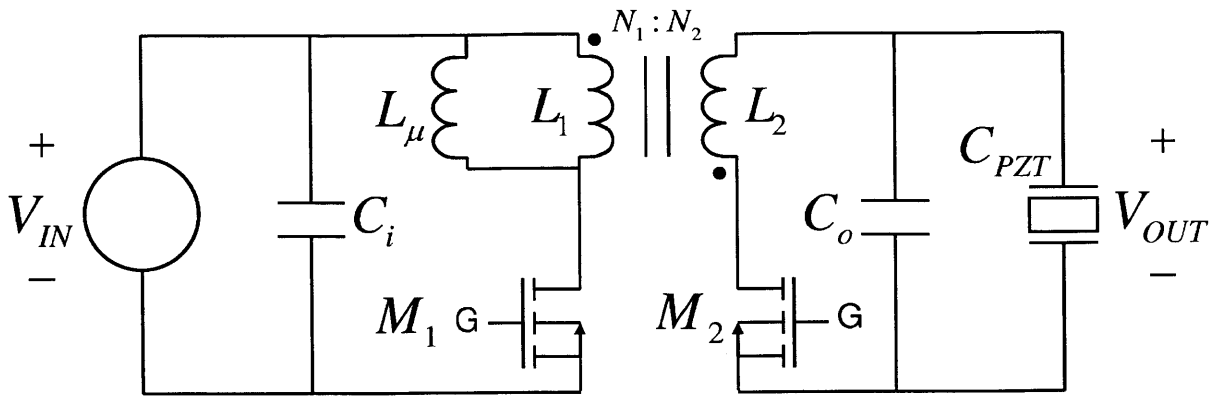

Figure 2-12: Bidirectional flyback converter with MOSFET switch implementation.

Transformer

Choosing the transformer requires not only consideration of the magnetizing inductance discussed above but also the turns ratio N_1:N_2 of the coils. The turns ratio of the coil determines the voltage load imposed on the low side MOSFET M_1 and the high side MOSFET M_2. Because of the turns ratio, the maximum voltage which must be supported by the switches is as follows:

$$V_{M_1} = V_{IN} + \frac{N_1}{N_2} V_{OUT}$$
$$V_{M_2} = V_{OUT} + \frac{N_2}{N_1} V_{IN}$$

The switch voltage stresses cannot exceed the maximum voltage rating of the MOSFET switches. The size of the switches can be increased to increase this voltage rating. However, as discussed before, the switches increased size will add mass the circuit, and the circuit mass must be carefully considered in the design. The transformer turns ratio also scales the currents flowing through each coil. Again, the maximum allowable current, which increases with increased MOSFET size, for the switches must be considered when choosing this turn ratio.

2.5.2 Closed-Loop Control Schemes

Need

The MOSFETs control the operation of the circuit and time the transfers of energy from one side of the circuit to the other. Thus, these MOSFETs must be properly controlled to allow proper functionality of the converter. The switches could potentially be controlled open loop. To charge the output, the low side MOSFET M_1 would be modulated driving energy to the output. To recover charge or harvest energy, the high side MOSFET M_2 would be modulated to drive energy back to the input. Then, only simple logic would be necessary to decide which mode the converter is in, and only simple hardware would be needed to actual supply the proper signals to the MOSFETs. This approach may be possible with certain output loads. For example, a proper switching frequency and duty ratio could be found to drive a stable, desired output voltage across a purely resistive load. However, finding this frequency and duty ratio is not possible when driving a purely capacitive load. Because a constant switching frequency and duty ratio delivers a constant amount of energy each cycle, driving this energy into a capacitance indefinitely would cause the capacitance to charge forever. For a real capacitor, the voltage across the capacitor would continue to increase until the capacitor's breakdown voltage was reached at which point the capacitor's dielectric would become conductive. This failure would cause a short and could destroy the capacitor. Because a PZT stack actuator essentially behaves as a capacitor electrically, this possible failure scenario is a very important consideration. Additionally, the PZT stacks have a maximum safe operating voltage. Continuous charging of the PZT capacitance could bring the stack voltage above this maximum which could lead to breakdown of the PZT material or other failure in the stack. Therefore, a closed-loop control scheme proves necessary to properly drive the PZT stacks. The output voltage must be fed back to a controller in some manner to alter the operation of the controller such that the output voltage can stabilize around a desired value. In the following, a possible closed-loop controller for this purpose is discussed.

Variable Frequency Control

Proposed by Karpelson et. al., one particular control scheme utilizes variable frequency and duty ratio cycles to achieve the desired output [4]. The details and required equations are describe in the above paper and its cited papers. In summary, the controller, as shown in 2-13, uses a comparator to determine when the high side switch voltage and the output voltage are equal. This condition means that there is no voltage across the secondary side of the transformer, and thus the current through this winding is constant. At this point, the output voltage is compared to the desired output voltage. These voltages determine a desired peak current which in turn determines an on-time for the necessary switch. Instead of calculating these numbers, a look-up table is used for speed. The high-side switch is used to discharge the load while the load side-switch is used to charge it. Because the on-time for the desired switch changes for each cycle, the control system natural adjusts the duty cycle and switching frequency to stabilize the load.

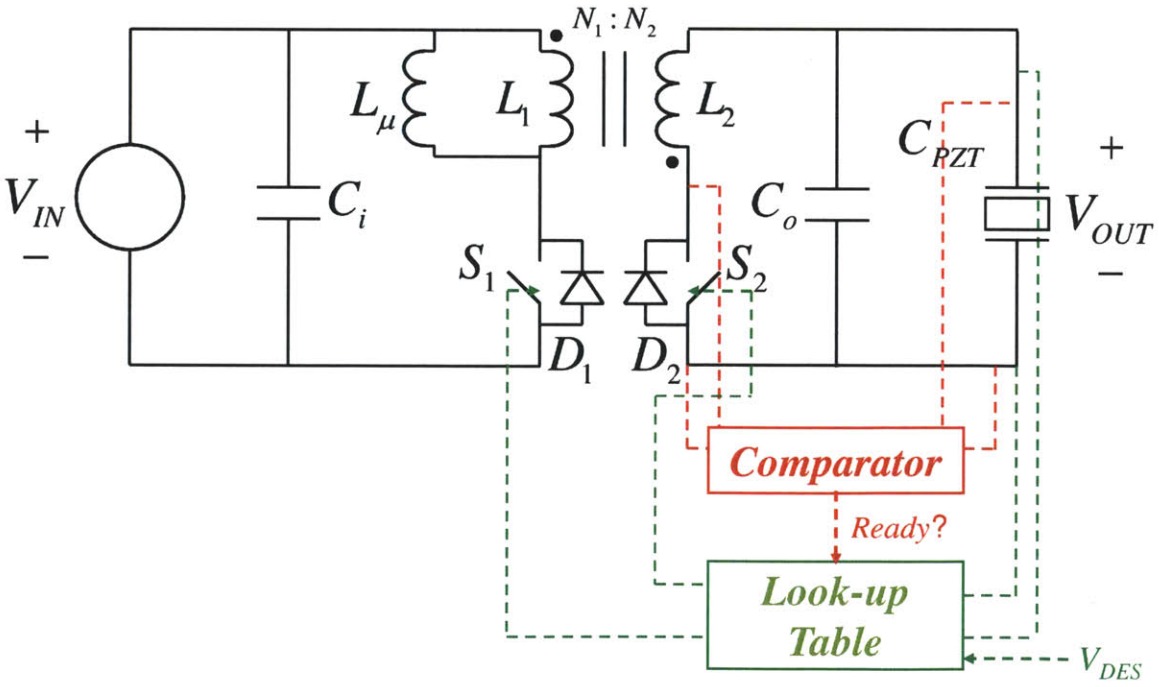

Figure 2-13: Bidirectional flyback converter with variable frequency control scheme.

2.5.3 Preliminary Results

As shown in 2-14, the bidirectional flyback converter was implemented on a solder board after designing the circuit to drive the PZT stack actuators:

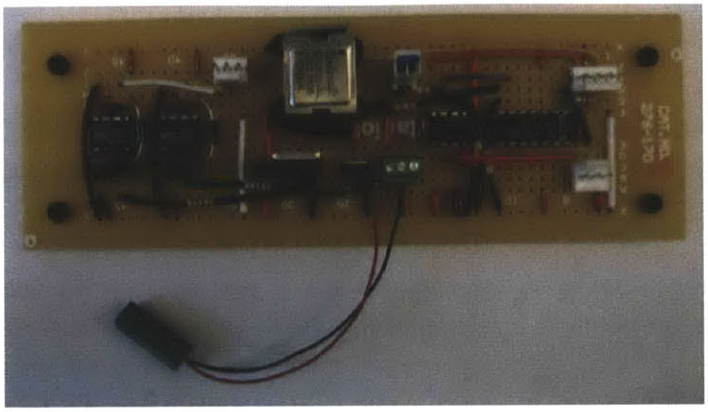

Figure 2-14: Solder board implementation of the bidirectional flyback converter with variable frequency control.

As described previously, the gate drivers (left of 2-14) drive the MOSFET switches (middle of 2-14) which control the energy transfer through the transformer (top middle of 2-14) which charges the PZT stack (bottom of 2-14). The instrumentation amplifier and comparator (right of 2-14) are used as components of the variable frequency control scheme described above. Not pictured in 2-14 is the National Instruments C-RIO 9074. This module interfaces with Labview software which allows the programming of an embedded field programmable gate array (FPGA) on the C-RIO. This hardware accepts inputs from the circuit, processes the control logic, and outputs command signals back to the circuit. Using the above circuit and variable frequency control scheme, the voltage output shown in 2-15 was produced. The top trace in the figure corresponds the output voltage V_{OUT} driving the output connected to a PZT to 100 [V]. The bottom trace corresponds to the voltage command sent to the low side gate driver to command the low side MOSFET's operation.

Although the trace shows an average output of approximately the desired output voltage, this signal has obvious high frequency oscillations when the voltage command given to the low side MOSFET goes low. This oscillation is due to parasitic effects

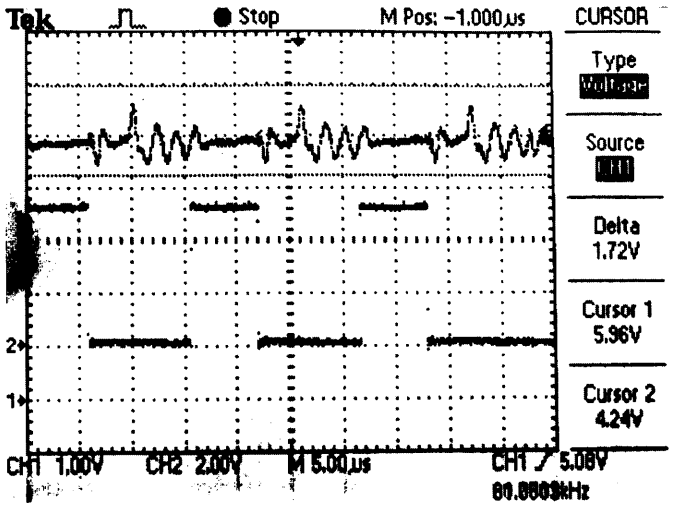

Figure 2-15: Preliminary output voltage results (top trace) with the low side gate drive signal (bottom trace).

in the MOSFET. These oscillations occur on time scales smaller than a single cycle. On much larger time scales, the controller properly drives the voltage output on the PZT. For example, 2-16 shows the circuit driving the PZT back and forth between 0 and 100 [V] at 1 [Hz].

The rising and falling edges of the square wave are not perfectly vertical because the converter cannot charge the PZT infinitely fast. The voltage rises over approximately 35 [ms] while the voltage falls over approximately 10 [ms]. This required charging time limits the maximum frequency at which the converter can be driven to 14.12 [Hz]. The charging time is controlled mainly by the peak current I_{pk} allowed through the transformer windings.

2.5.4 Shifting Desired Functionality

Although this converter topology seemed promising, the complexity of the design and control created problems. The topology seems more appropriate for higher power applications which would warrant active control. A design could be made for this application, but after some iterations, the difficulty of this approach made this topology undesirable. Furthermore, a very small amount of energy was available to harvest even with substantial loads applied to the PZT cell. Without a practical desire to har-

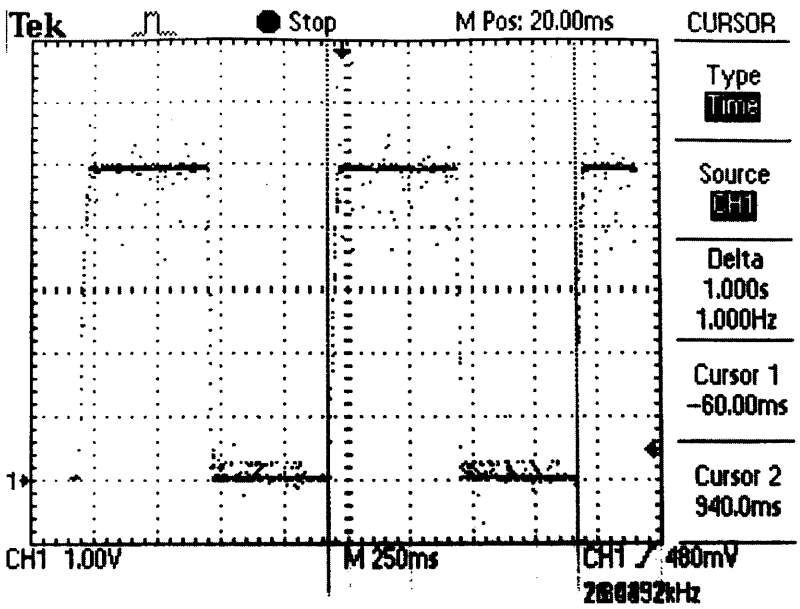

Figure 2-16: PZT stack driven by bidirectional flyback converter from 0 to 100 [V] at 1 [Hz].

vest energy, the remaining functionalities of drive and charge recovery could also be addressed with different, simpler topologies which do not require precise active control and high-frequency switching. Thus, the bidirectional flyback converter topology was abandoned. 3 describes a new direction and a different approach to the original goal of this work.

Chapter 3

Distributed Actuation

3.1 Background

A novel method to coordinate groups of PZT-based actuators for large scale actuation is discussed in the following. Lead Zirconate Titanate (PZT) is a material which changes shape based on an applied voltage. The strain of PZT material is relatively small while the output force is relatively large. PZT stacks which will be utilized in this design are comprised of many layers of this material in series to increase the overall strain. Each stack has a maximum displacement of $\sim$40 [μm] with a force of 850 [N] at 150 [V].

The stack strain is still insufficient for purposes of large scale actuation. Researchers at the D'Arbeloff Laboratory at the Massachusetts Institute of Technology have developed multiple ways using mechanical flexures to increase the strain $\sim$100 fold while attenuating the output force by a factor of $\sim$100. The PZT stack setup with this mechanical amplification will be referred to as a PZT cell.

An unloaded PZT stack approximately behaves electrically as a capacitor. Initial charge is needed to cause the stack to elongate, and this charge must be removed to relax the stack. The stack does not need continuous input current to hold its elongation. To remove the charge from the stack, the inputs of the stack can be shorted together to dissipate the energy. However, the energy on the stack could also be transferred to another medium for later use. The latter option can allow for a

much more efficient system if the stack energy can be efficiently reused.

3.2 Actuator Design

Many PZT cells with coordinated activation will be distributed on a mechanical load to produce a desired motion. A linear actuator will be used to illustrate the concept although the concept can be directly applied to a rotary actuator in the same manner.

As shown in 3-1 below, n PZT cells are mechanically coupled to a gear tooth such that their elongation can apply force to the sloped surface of the gear tooth causing gear motion horizontally. Depending on the spacing of the cells compared to the pitch of the gear, the desired motion direction, and the desired gear speed, the activation of the different cells will generally occur at different times. That is the activation of one cell, while following the same voltage profile as all of the cells, will be phase shifted in time from the activation of other cells.

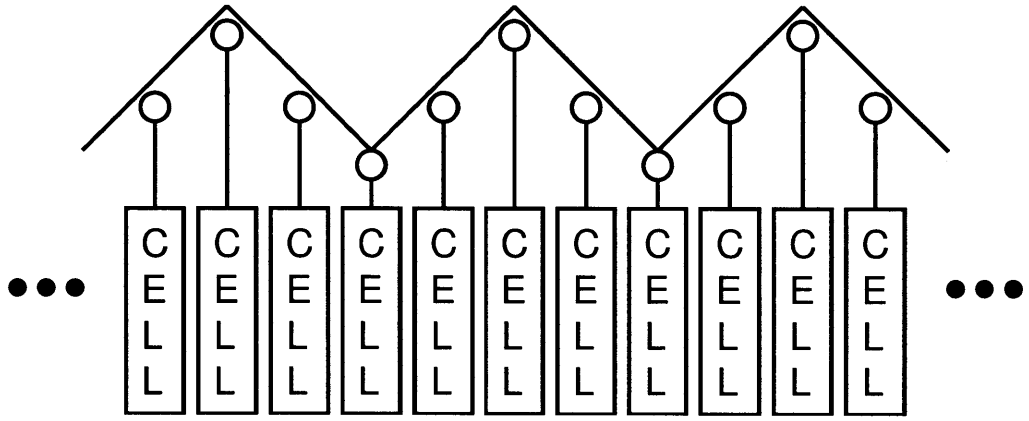

Figure 3-1: PZT cells mechanically coupled to gear tooth to drive a desired motion.

Depending on the desired actuation profile, the n PZT cells will be separated into m groups. In general, the PZT cells in each group need not be physically adjacent. Each of the m groups will be paired with another group that's desired activation is 180° out of phase. Therefore, only one group in these $m/2$ group pairs will be activated at one time. However, one group of the pair is always activated. Therefore, at any time, $m/2$ groups of cells in the actuator are activated while the others are deactivated. To charge the cells in a group together, the individual cells will be connected in

parallel electrically. Parallel electrical connection avoids requiring extremely high voltages from the power source to drive a large number of serially connected PZT cells which each require a input voltage near 150 [V].

For simplicity in the following discussion, each group in each pair will be considered to be comprised of only one PZT cell. However, in general a pair could contain multiple PZT cells in each group.

Because only one cell in each pair is activated at a time, the properties of PZT can be exploited to increase the efficiency of the actuator. To achieve this, the charge from one cell is transferred through appropriate circuitry to the other to deactivate the first cell in the pair and activate the second. This process can be repeated in reverse to deactivate the second cell and reactivate the first cell.

Then, depending on the desired actuator direction and speed and the mechanical design including the actuator placement and gear design, the m groups are properly coordinated to produce the desired motion. The coordination entails properly choosing the phase difference between the activations of the various groups to cause the proper aggregate output motion of the gear. The coordination of the various transfers of energy can be coordinated by a controller which governs the entire system. This controller would determine the time to transfer charge from one cell to another and also control the phase shifts between the transfers of various groups.

In this way, charge used to activate one PZT cell can be reused to activate another. If the transfer process were perfectly efficient and no output work was performed, once $m/2$ cells were activated, the current charge in the actuator could remain indefinitely activating different cells as it was transferred from one to another. However, because the system inherently does mechanical work on the gear and the load it drives and because perfect efficiency and a perfectly efficient charge transfer are impossible in reality, additional energy must be added to the system over time to keep the actuator operating at any desired level.

3.3 System Overview Diagram

3-2 shows an overview of the system in block diagram form. The m groups of PZT cells interact with the mechanical domain through the particular mechanical design of the actuator. These PZT cells receive their power from the energy stored in a battery. The battery power is brought to the cells through some power transfer circuitry which is also designed to allow power to be transferred from one PZT cell in the $m/2$ pairs of cells to the other. Therefore, this circuitry must meet three functional requirements: 1) initially charge the required PZT cells, 2) allow charge to transfer between each cell in a pair, 3) impose full activated and deactivated voltages if full energy transfer does not occur. The final component of the system is the controller which coordinates the movement of charge. The coordinator controls the type of energy (battery to cell, cell to cell, or cell to cell with battery compensation) that must occur and controls the timing of the charge transfers to produce the desired mechanical output of the system. The coordinator commands the proper phase differences in the charging and discharging waveforms for the m cells in the actuator.

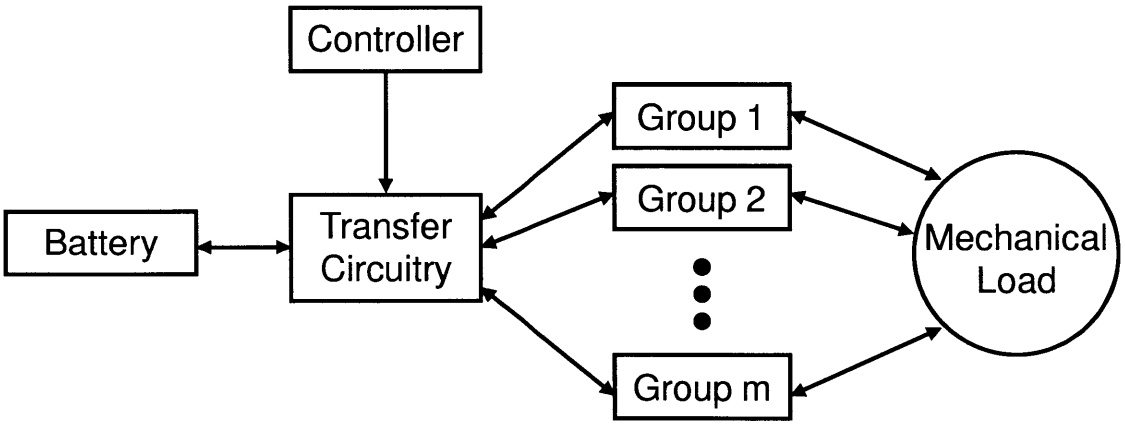

Figure 3-2: Block diagram of the overall system architecture for the PZT driven actuator.

3.4 Possible Transfer Circuitry

Campolo, Sitti, and Fearing have proposed a possible circuit to accomplish the power transfer requirements listed above [3]. 3-3 shows the schematic of the proposed circuit.

The power transfer from one cell to another in one of the $m/2$ pairs is accomplished by connecting the charged cell's capacitance through and inductor and a diode to the other cell's capacitance. The inductor allows a full charge transfer to occur between the capacitances that would not be possible by simply connecting the capacitors together. Using the inductor also avoids a loss of have of the energy inherent in directly charging a capacitor. The diode prevents the LC tank created from allowing any charge to transfer back to the originally charged PZT capacitance. With no losses, this scheme can have a 100% efficient charge transfer from one cell to the other.

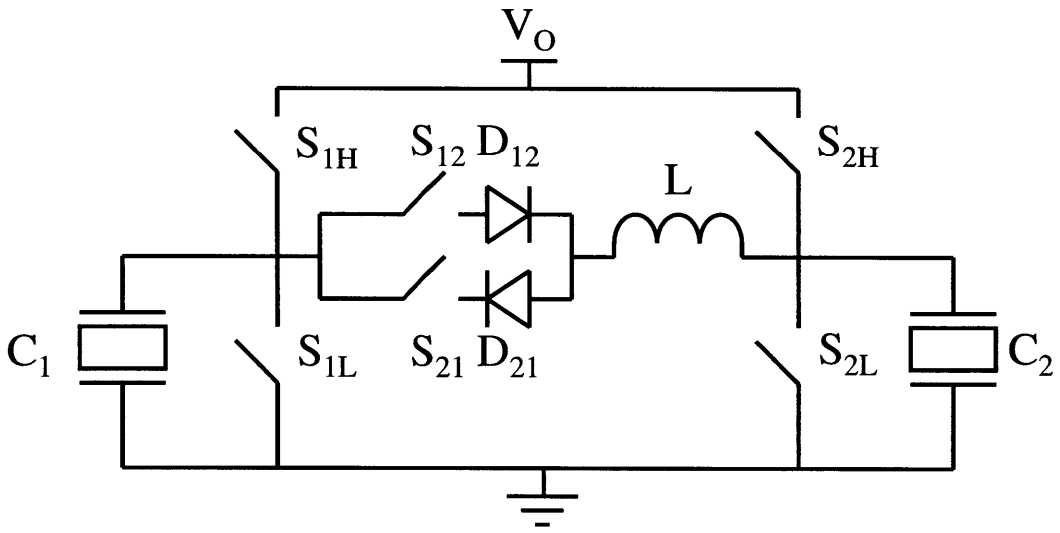

Figure 3-3: Possible circuitry for PZT charging, charge transfer, and loss compensation.

With losses and the diode forward voltage, the transfer will not fully charge the second PZT cell. The extra switches in the system connect to the power and ground rails which can finish charging the PZT to compensate for lost energy and an incomplete charge transfer. Each cell can be charged individually. Also, if either capacitance is completely discharge as it would be initially, the PZT cell's capacitance can be connected to the power rail to initially fully charge one of the cells in the pair. Therefore, this circuit can fulfill all the required criteria for the power transfer block. Each of the $m/2$ pairs of PZT cells would require one such circuit between them for this functionality. The controller block would need to properly coordinate the switches in the

above circuit and between the various circuits in the system to achieve the desired mechanical output.

3-4 shows the switch timing diagram for cell-to-cell energy transfers and the corresponding voltages on the two PZT cells. In each cycle, S_{1H} closes to fill the charge on C_1 while S_{2L} closes to discharge C_2. After both switches open, the voltages remain on the cells until the transfer occurs. S_{12} closes to transfer the charge from C_1 to C_2. Then, S_{2H} closes to fill the charge on C_2 while S_{1L} closes to discharge C_1. At this point, C_1 and C_2 have simple switched roles and the symmetric sequence of switch states occurs until the system returns to its original state. The length of the hold depends on the necessary mechanical actuation frequency to create the desired actuator motion.

Additionally, the circuit operation eliminates chances of large voltages spikes due to disconnecting the inductor from the circuit which sometimes causes complication in similar circuits. The diodes in the circuit cause the cell voltages to remain constant after the transfer with current no longer flowing in the circuit. At this point, the inductor is disconnected requiring that inductor current is zero. Because the inductor current was already zero before it was disconnected, no change in current occurs, and thus no spikes occur in the inductor voltage.

3.5 Shared Inductor Option

Although the above discussion has concentrated on each of the $m/2$ pairs being comprised of only two PZT cells, the general case for the actuator could have multiple PZT cells in each of the m groups and two such groups in each of the $m/2$ group pairs. Again, to charge the cells in a group together and avoid requiring an extremely large input voltage, the individual cells will be connected in parallel electrically. Depending on the number of cells per group, the total capacitance of a group charged in parallel can become large on the order of 100 [μF]. With all other parameters constant, increasing the size of the inductance L without increasing the inductors series resistance can significantly improve the cell group to cell group transfer efficiency. To

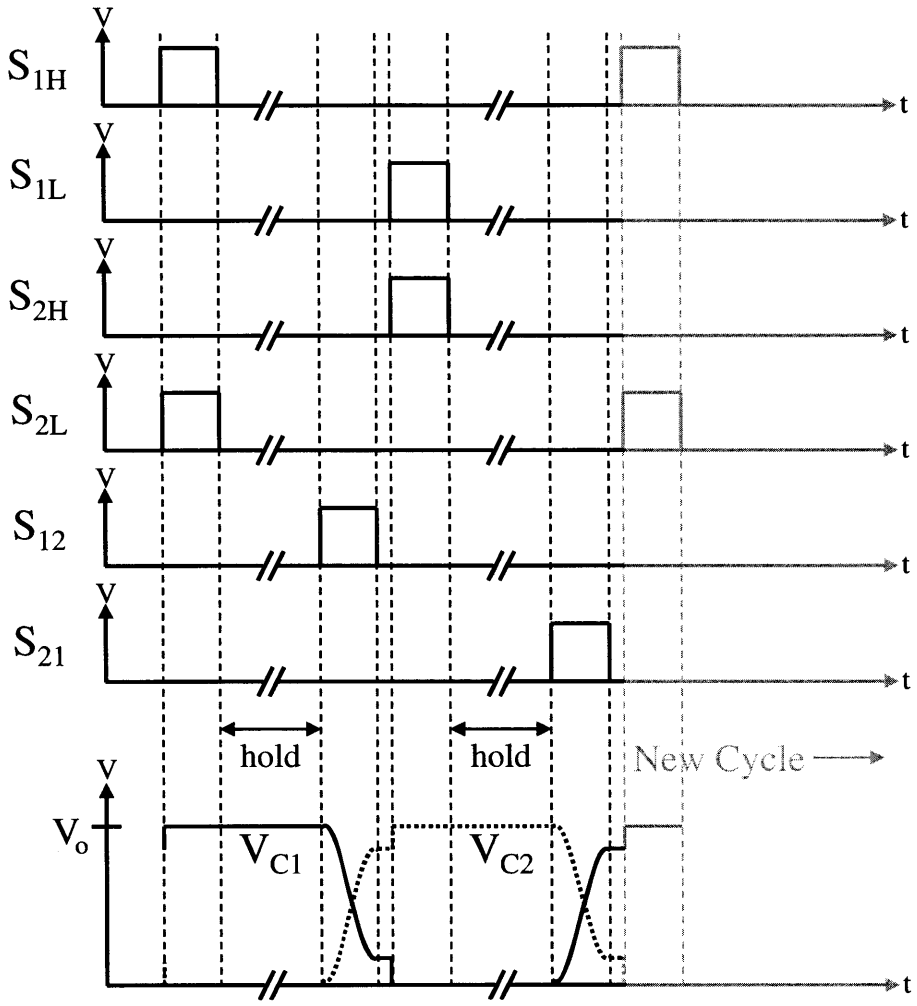

Figure 3-4: Switch timing diagram and corresponding cell voltages for charge transfer cycle.

achieve these requirements, the inductor must become physically larger in general.

For certain actuator designs, the size and weight of the multiple inductors needed may become prohibitive. However, by sharing a smaller subset of inductors, the actuator can achieve the same functionality with less size and weight. Adding more switches which link separate group pairs, one inductor could be used for multiple pairs. Sharing an inductor would not allow charge transfers in the separate pairs to occur simultaneously. However, because the speed of the charge transfer is significantly faster the mechanical frequencies of actuation, more advanced coordination between the cells can still achieve the same functionality outlined above. If two pairs must transfer charge at nearly the same time, the circuit could perform one charged transfer followed by the next. Then, because the characteristic time of the transfers is so much shorter than the characteristic time of the mechanical motion, the ordered rather than simultaneous transfers would be inconsequential.

In some cases, the choices of parameters may cause the electrical transfer frequency to not be sufficiently higher than the desired mechanical frequency. Without a large frequency difference, multiple cell pairs could not undergo a transfer one after another with the total time of all transfers remaining sufficiently small compared to the mechanical time constants. In this way, the cascading of the transfers would be noticed which would violate the nearly simultaneous assumption needed to generate the appropriate actuator behavior. In these cases, additional inductors can be used with certain pairs assigned to each inductor. Weight and size savings can still be achieved as long as the number of inductors is less than one for each pair. For example, four inductors could be used. The $m/2$ pairs would then be separated into 4 groups each assigned to its own inductor.

3-5 shows the same circuit as 3-3 with two extra selection switches S_{sel1} and S_{sel2} added. The figure is only shown with two cells to avoid clutter. However, the selection switches of each pair of cells would connect the cells to the same left and right terminals of the transfer unit. The transfer unit in the center of the diagram would be shared by all cells. The selection switches would choose which pair was connected to the transfer unit at any point. Therefore, only a single inductor and set

of diodes would be used for all of the cell-to-cell energy transfers.

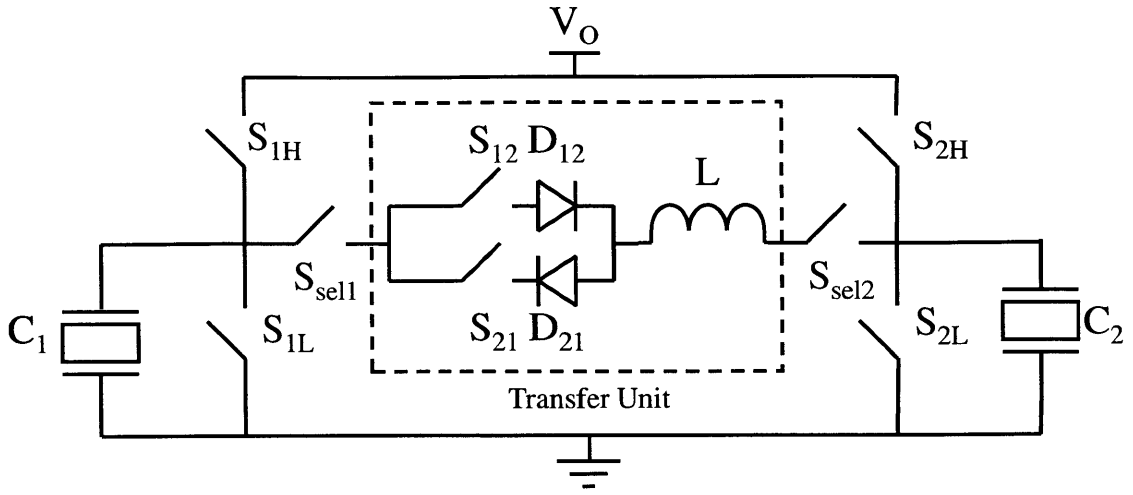

Figure 3-5: Drive circuitry with extra selection switches.

In 3-3, each circuit for a pair of cells required 6 switches. Adding the selection switches still requires 6 switches per pair only adding the two extra switches in the transfer unit to the total switch count. Therefore, the use of selection switches only causes a constant increase of 2 switches and not an increase of switches in proportion to the number of cells.

Additionally, the use of selection switches also allows the circuitry to change which cells are paired at any given time. Although some situations may not require a change in the cell pairings, the selection switches allow this functionality which may useful for certain applications.

3.6 Circuit Implementation

The implementation of the circuit in 3-3 requires special care to properly implement the switches controllable by a microcontroller or similar device. The circuit switches consist of two half-bridges and two switches connecting those half-bridges. However, only switches S_{1L} and S_{2L} have a ground referenced node. A simple gate-driver chip can control NMOSFETs for these switches. However, special care is needed to properly implement and drive the other four switches.

As shown in 3-6, the Fairchild FAN7390 gate driver was chosen to drive each half bridge. However, because the load connected at the center of the half bridge, the PZT actuators, is capacitive, using a NMOS for the top switches S_{1H} and S_{2H} is not possible. With both switches off, the configuration of the circuit for two NMOSs in the half-bridge would cause the capacitive load to charge to the chip supply voltage because the load creates a path to ground from that voltage supply. Thus, the load could never float at a given voltage which is a necessary requirement of the circuit. Instead to take advantage of the switches connection to the high-voltage rail, PMOSs was used for S_{1H} and S_{2H} with the addition of 15 [V] Zener diodes and current-limiting resistors.

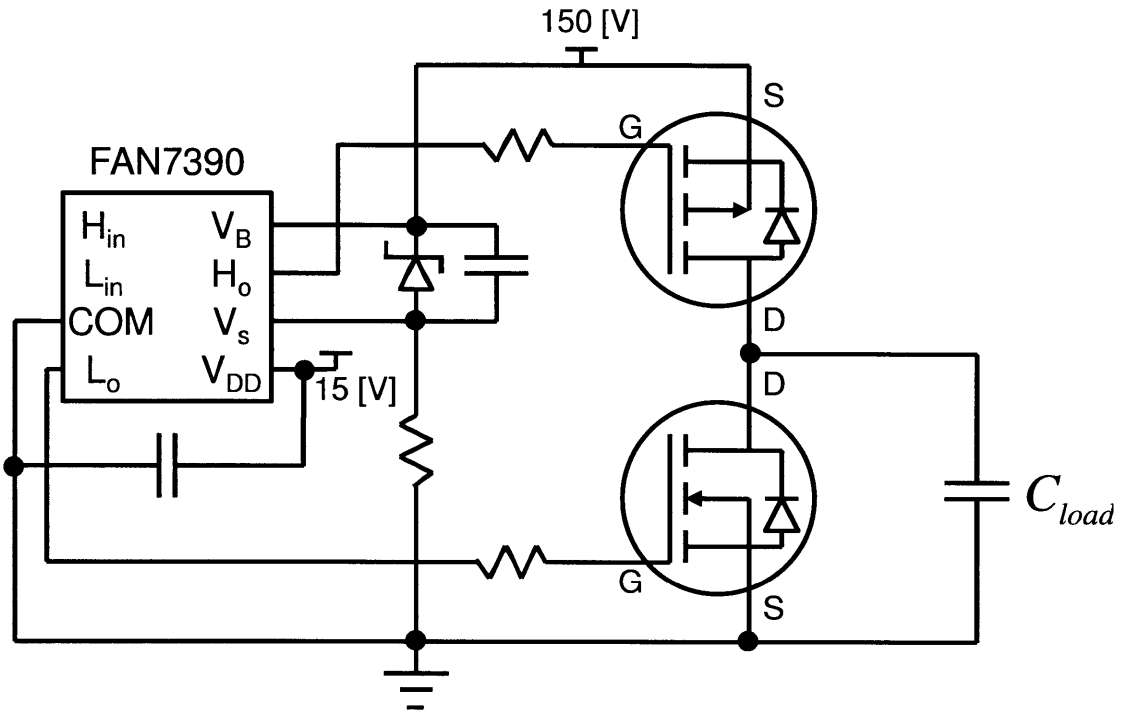

Figure 3-6: Half-bridge switch circuit implementation using both NMOS and PMOS.

The floating switches S_{12} and S_{21} which connect both half bridges have no connection to either rail in the circuit. A circuit using two NMOSs and a gate-driver chip can be used for each switch. However, similar to the two NMOS half-bridge, the connection of a capacitive load causes a problem. In this instance, driving these switches in this manner necessarily drains energy from load, again, not allowing the voltage to float. The simplest method to solve this problem is utilizing opto-couplers for these

switches. This method is undesirable because opto-couplers require significantly more power than MOSFETs. However, because these switches only need to be active for short periods of time, the power consumed compared to the power transferred for the desired application space is small. 3-7 shows the implementation of the floating switches S_{12} and S_{21}.

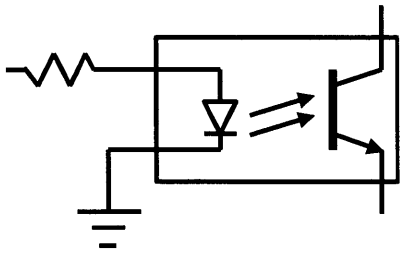

Figure 3-7: Floating switch implementation using opto-coupler.

3-8 shows a full schematic for the circuit in 3-3 using the above mentioned switch implementations. One half-bridge and PZT capacitance is connected through the opto-couplers and the inductor to the other half-bridge and PZT capacitance. A controller is used to control and synchronize the switches according to the switching diagram in 3-4. The high-voltage rail can be supplied using a standard DC-DC boost converter with a battery as an energy source. Similarly, the battery can be directly connected to the chip supply voltage or another appropriate DC-DC converter can be used to supply this voltage.

3.7 Preliminary Experimental Results for Circuit

3-9 shows voltage signals for two PZT cell banks utilized as the capacitive loads in the circuit above. For this experiment, 40 [V] was used as the high rail to avoid fatiguing the PZT cells unnecessarily. However, this circuit implementation and fabrication is capable of supporting high-rail voltages of 200 [V]. Each cell bank has the same capacitance of $C = 5.6$ [μF], and the circuit uses an inductor with $L = 100$ [mH]. The cell banks initially start at each voltage rail approximately. The circuit moves the charge from one cell bank to the other during the transition period. For the sake of clarity, the voltages float momentarily and then are pulled to the opposite rails from

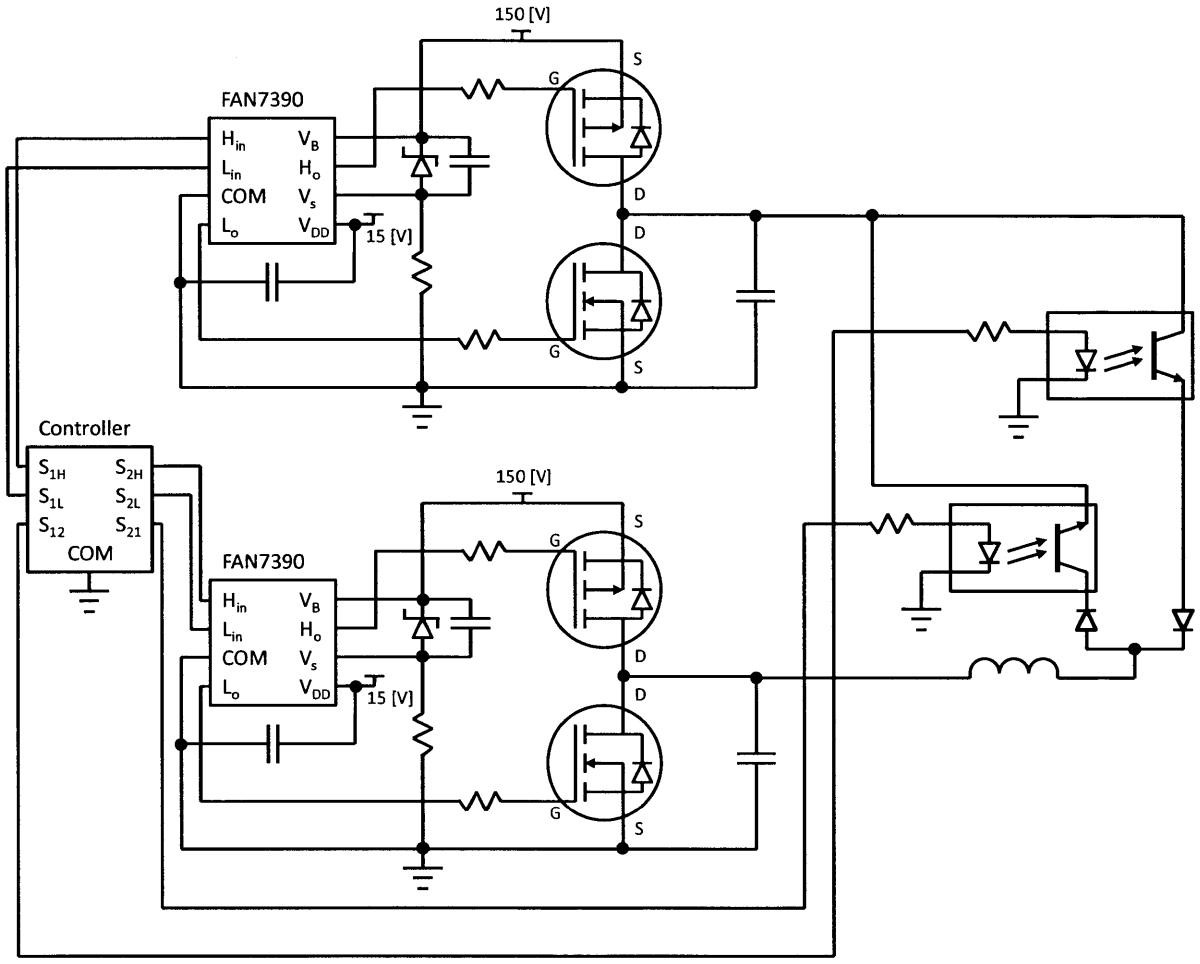

Figure 3-8: Full circuit implementation of 3-3.

which they started. Thus, the circuit exhibits the behavior desired and discussed above.

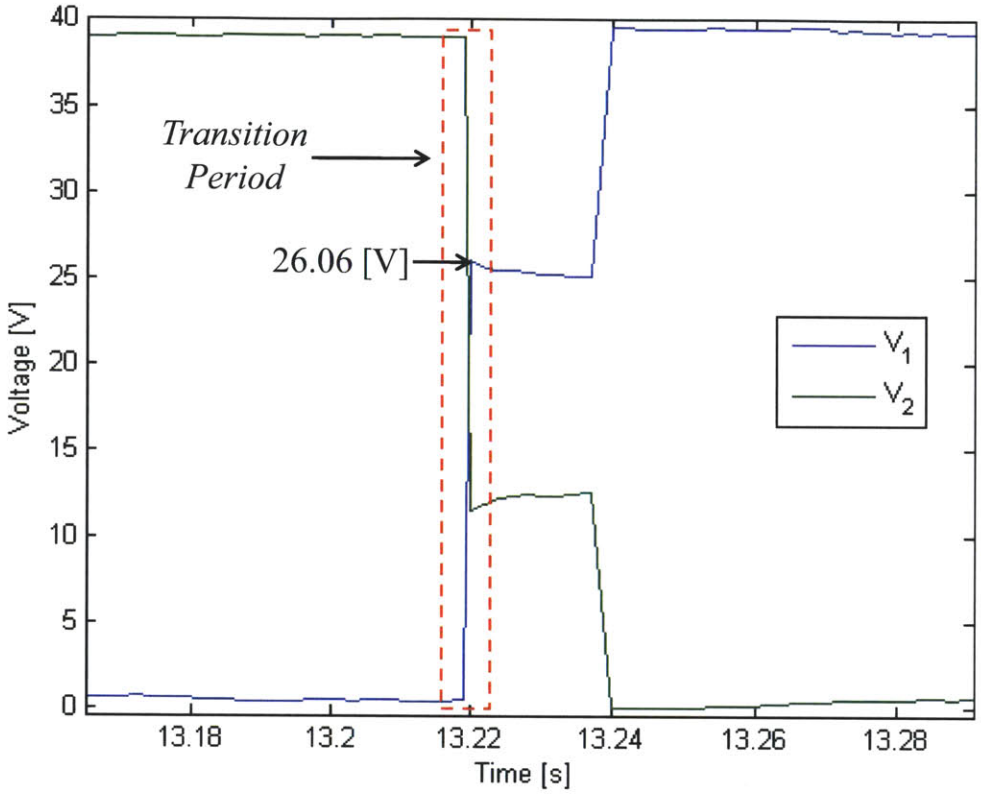

Figure 3-9: Preliminary experimental result for circuit with no optimization.

Comparing the energy usage of this circuit versus standard drive circuitry reveals the effectiveness of the circuit. A standard way to drive the actuators would be to charge one bank and discharge it and then to charge the other cell bank and then discharge it. With or without transferring charge between the cell banks, the cells must be able to connect to both voltage rails. Therefore, the half-bridge circuitry used in the experiment would be necessary even if driving the actuators in the standard way. In the following energy calculations, the energy required to drive the half-bridges is ignored as this energy would be used in both situations. Then, the energy per cycle with no transfer would be

$$E_{NT} = CV_o^2$$

while the energy with transfer would be

$$E_T = C(V_o^2 - V_H^2) + P_{ON}T$$

where V_H is the voltage recovered to the recipient cell bank after a transfer, P_{ON} is the opto-coupler power and equals 0.024 [W], and T is the period of the LC circuit created during a transfer and equals $2\pi\sqrt{2LC}$. The percentage of energy saved would be the ratio of the energy used in the circuit described above to the energy used in the standard drive circuit.

$$\%E_{save} = 100\frac{E_T}{E_{NT}}$$

In this implementation, E_{save} is 40.7 %. This percentage will be the same percentage of power saved at a given frequency between the two drive strategies. Besides the constant offset of the opto-coupler power, this percentage will be the same even when higher voltages are used for the top rail. Although this implementation shows significant energy savings, the circuit has not been optimized in any way. With optimization, this percentage could be increased significantly. Because the energy scales as voltage squared, a percentage increase in the recovered voltage will lead to a larger percentage increase in the energy saved. As cell bank capacitance increases, because of more PZT cells or larger PZTs, the energy used by the opto-coupler will become more negligible. Using the above relationships,

$$\%E_{save} = 100\frac{CV_o^2 - (C(V_o^2 - V_H^2) + P_{ON}T)}{CV_o^2} = 100\frac{CV_H^2 - P_{ON}T}{CV_o^2}$$

Rewriting T in terms of C,

$$\%E_{save} = 100\frac{CV_H^2 - P_{ON}2\pi\sqrt{2LC}}{CV_o^2}$$

As C increases, the fraction $P_{ON}T/CV_o^2$ goes to zero. Quickly, this term becomes negligible compared to the first term in the equation. For example, with a gear driven by 10 cells in each bank, 20 cells total, $P_{ON}T = 0.00036$ [J] while $CV_H^2 = 0.01893$, the

later of being approximately two orders of magnitude larger. Therefore, with systems even on this scale, the percentage of the energy recovered will scale with the square of the percentage of the voltage recovered. Letting R_{Vrec} denote the fraction of the voltage recovered,

$$\%E_{save} = 100\left(\frac{V_H}{V_o}\right)^2 = 100\left(\frac{R_{Vrec}V_o}{V_o}\right)^2 = 100R_{Vrec}^2$$

This equation suggests that optimizing the circuit should simply be an attempt to drive the recovered voltage V_H as high as possible compared to the high voltage V_o. An optimized circuit must also use an inductive element when charging the PZT cells from the high-voltage rail. Many standard designs and DC-DC converters exist with inductive elements to supply the high-voltage rail. Although ignored in the circuit diagram and analysis, care must be taken to ensure that the circuit sourcing power to the high rail does so through and inductive element to avoid the immediate loss of energy equal to the energy sourced to the PZT capacitance. This phenomena occurs with direct capacitor charging from a voltage source and is well documented.

3.8 Generalized PZT Driven Linear Actuator Model

The development of this model aims to explore the characteristics of a distributed interaction between PZT cells and a linear gear. The PZT cell model is developed first to show the two-way transforming nature of the PZT. As shown in 3-10, the model has a electrical and mechanical domain. The two domains are coupled by the piezoelectric effect. The mechanical domain is represented by a lumped mass with a spring and damper tied from the mass to ground. Through the piezoelectric effect, a force is exerted on the mass proportional to the voltage on the PZT. The net motion of the mass is coupled to the load through a lever arm which represents the flexure system. The displacement of the mass is amplified by G_f while the transmitted force is attenuated by the same constant. The electrical domain has a PZT capacitance in parallel with a dependent current source. Again, through the piezoelectric effect, the displacement of the mass causes a current from the dependent current source. A

voltage source is in parallel with both of these elements. This voltage source drives the PZT and, with the other PZT cells, the entire system.

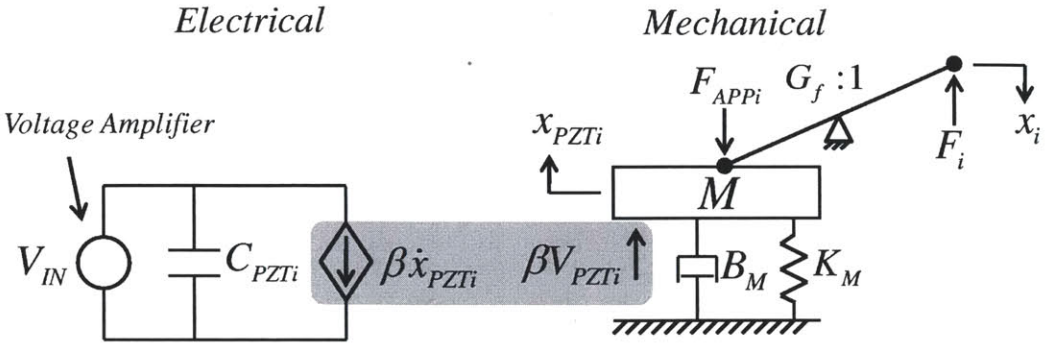

Figure 3-10: Lumped-parameter model of the PZT cell.

This model can be represented as a single differential equation relating PZT voltage and cell's output force to the cell's output motion. Then, using experimental data as well as parameter measurements and estimations, the following equation can correctly predict the behavior of a single PZT cell.

$$\frac{\beta}{G_f}V_{PZTi} - \frac{1}{G_f^2}(M\ddot{x}_i + B_M\dot{x}_i + K_M x_i) = F_i$$

3-11 shows the model of the gear system with the PZT cells pushing against the teeth of a linear gear. The gear is modeled as a lumped mass M_g and damping b with a particular shape $z = f(y)$ as defined in the figure. The initial positions of the PZT cells are donated y_{io}. For evaluation purposes, the model also defines y_i as the relative position of the cells once the gear has moved some distance y_g. The cells do not actually move in the system, but this definition allows easy evaluation of the gear shape and its derivatives at the position of the PZT cells after some motion. Just as in 3-10, the force and displacement of each PZT cell is denoted F_i and x_i respectively. Finally, a general external force F_{ext} is included to model a constant external load on the linear actuator.

With the PZT cell forces and external force as inputs, the gear model can be written in a differential equation relating the PZT cell forces to the motion of the gear. To do this, the PZT cell interaction with the gear teeth must be carefully

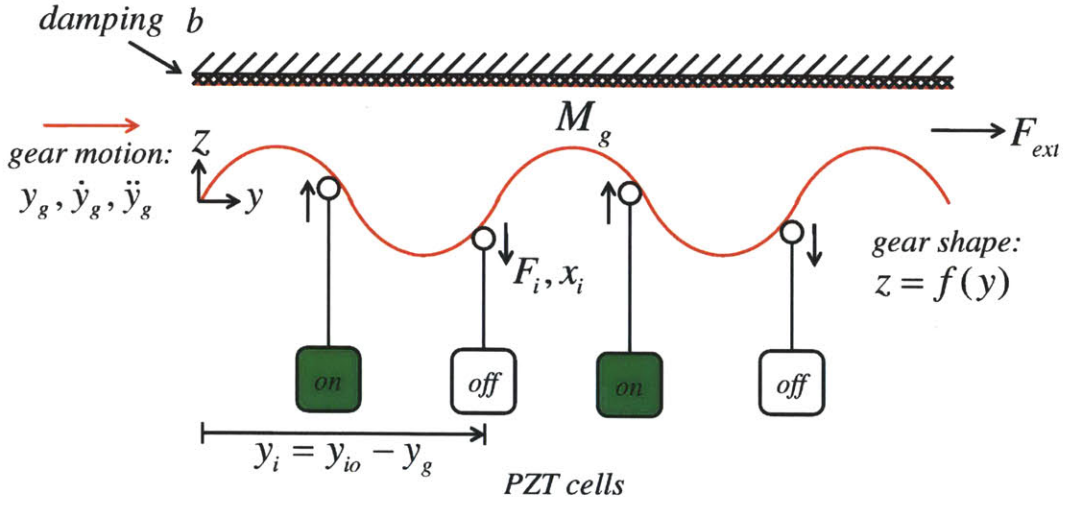

Figure 3-11: Lumped-parameter model of the PZT cells' interaction with a gear.

considered. 3-12 shows a close view of a small section of the gear tooth where the PZT cell may be interacting.

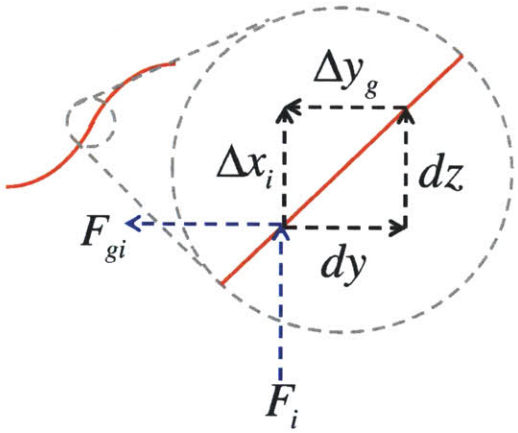

Figure 3-12: Close up view of section of a gear tooth.

Considering small displacements in this region,

$$\frac{\Delta x_i}{\Delta y_g} = -\left.\frac{dz}{dy}\right|_{y_i}$$

This equation directly leads to

$$\dot{x}_i = -\left.\frac{dz}{dy}\right|_{y_i} \dot{y}_g$$

Then, with the assumption that power is conserved

$$F_i \dot{x}_i = F_{gi} \dot{y}_g$$

which leads to

$$F_{gi} = -\left.\frac{dz}{dy}\right|_{y_i} F$$

With these two interaction relationships, the gear model, and then the full model, can be developed with the parameters of the equation dependent on the shape of the gear and its spatial derivatives. For the gear,

$$M_g \ddot{y}_g = -\sum_i \left.\frac{dz}{dy}\right|_{y_i} F_i - b\dot{y}_g + F_{ext}$$

Combining the two model equations and appropriately relating the displacement of each cell to the gear displacement yields

$$\ddot{y}_g = E(A\dot{y}_g^2 - B\dot{y}_g + C - D + F_{ext})$$

where

$$A = \frac{1}{G_f^2} M \sum_i z' z''$$

$$B = b + \frac{1}{G_f^2} B_M \sum_i (z')^2$$

$$C = \frac{1}{G_f^2} K_M \sum_i z' z$$

$$D = \frac{1}{G_f} \beta \sum_i z' V_{PZTi}$$

$$E = \frac{1}{M_g + \frac{1}{G_f^2} M \sum_i (z')^2}$$

where

$$z = z(y_i)$$

$$z' = \frac{dz(y_i)}{dy_i}$$

$$z'' = \frac{d^2z(y_i)}{dy_i{}^2}$$

and

$$y_i = y_{io} - y_g$$

3.9 Simulation Results

The full generalized model was implemented in MATLAB to simulate the system. Numerical integration was necessary to simulate the response of the time-varying, nonlinear system. The nature of the equations leads to large variations in the derivatives. The numerical results show some oscillations in velocity around an average value, and thus, averages of this signal was considered.

Certain system components were set arbitrarily to allow initial observation of the system characteristics. First, the gear shape was set as a sinusoid with amplitude A_g = 0.8 [mm] and gear period, or pitch, $T_g = 2\pi A_g$ [s]. The gear amplitude must be less than the dynamic stroke of the actuator. Second, four PZT cells spaced by half of the gear pitch T_g between each were used in the initial simulations although the simulation can be scaled to an arbitrary number of cells. Third, some desired voltage signal must be fed to each cell to cause gear motion. For simplicity, a controller was implemented which activates all PZT cells which will aid the gears motion in the desired direction and deactivates any cells which will impede. In some sense, this scheme will simply try to drive the gear as fast as possible. Thus, the controller does not give useful control for many circumstances but simply provides a useful basis to be exploration of the model. In a physical implementation, this scheme would only require a position sensor and knowledge of the gear shape and thus is entirely

practical.

3-13 shows the displacement and velocity signals over a 4 [s] period with gear damping $b = 0$ $[\frac{Ns}{m}]$, gear mass $M_g = 0.5$ [kg], and external force $F_{ext} = 0$ [N]. The simulation shows an average no-load speed $\dot{y}_{gss} = 2.4$ $[\frac{m}{s}]$.

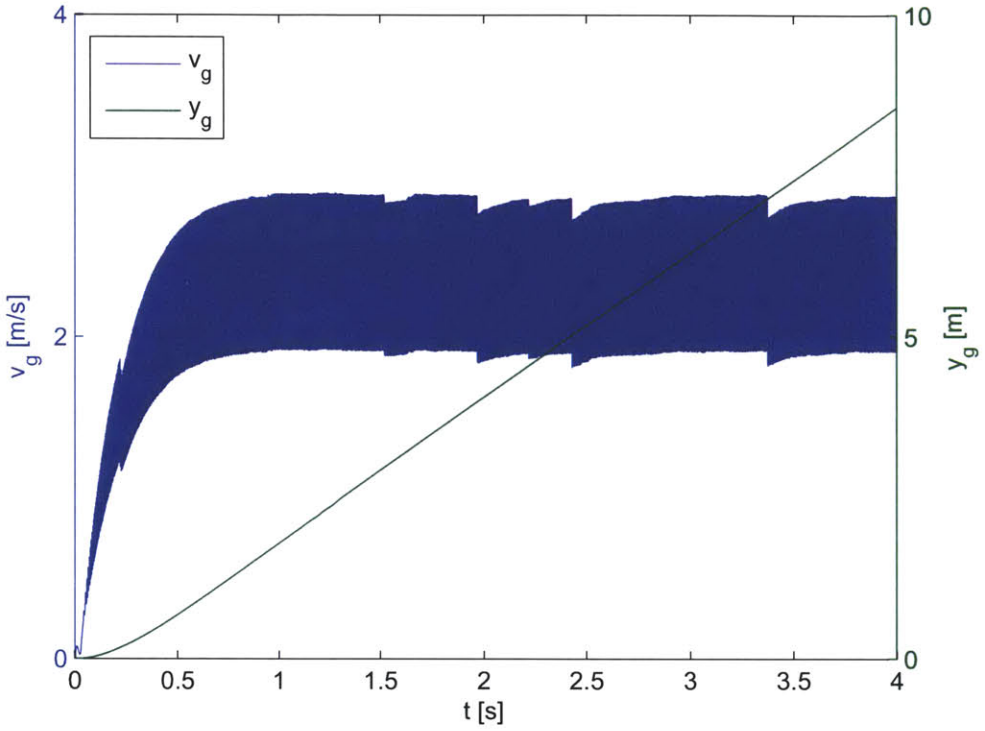

Figure 3-13: Position and speed of the gear over time actuated by two sets of two PZT cells driven 180° out of phase.

For verification purposes, an animation was created to visually inspect the motion to ensure a reasonable solution from the numerical integration. A frame from this animation is shown in 3-14.

The stall force of an actuator is another important metric. However, the stall force must be carefully considered in the arbitrary setup of the simulation. Normally, finding the stall force requires applying sufficient external force until the gear does not move when starting from rest. For four PZT cells with only two acting at any one time, this stall force $F_{Sext} = 14.4$ [N] and scales linearly with the number of cells

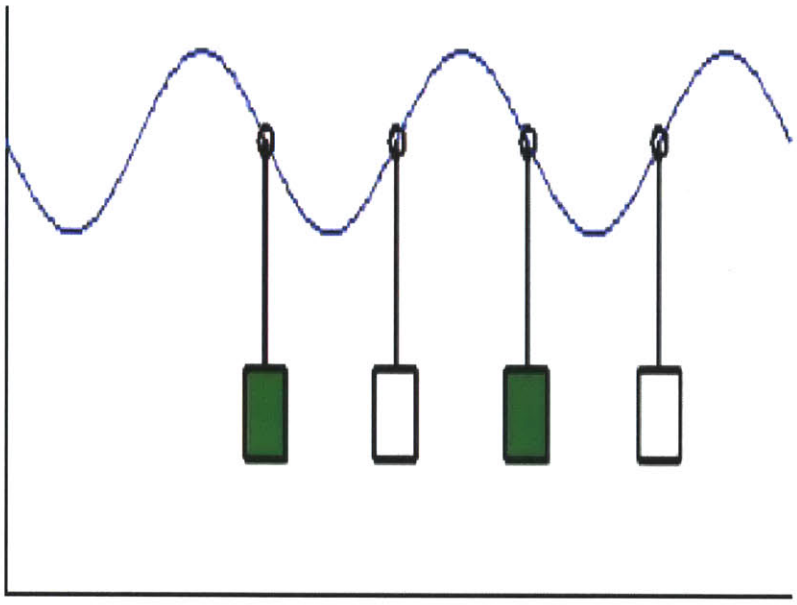

Figure 3-14: Frame of the animation of the gear motion.

used. However, spacing the cells a half pitch length apart relies on the motors inertia to pass the gear through the singularity where the slope of the tooth is zero. After passing through this point, the next set of cells can activate and continue moving the gear. Thus, with external forces much smaller than the stall forces, the gear does not maintain enough inertia to pass through the singularity and thus no steady state speed is every reached although the gear does move initially. This phenomenon is entirely dependent on the cell spacing. For example, spacing the cells closer together would allow more cells to aid the gear motion without relying solely on the gears inertia and thus avoid this problem to some degree. Another similar solution would be space the PZT cells farther apart such that the same result occurs. Therefore, a meaningful measurement of the stall force would highly depend on the desired cell configuration and is not well represented with the arbitrary choices in this initial simulation.

3.10 Future Physical Implementation

A physical prototype of PZT cell driven gear will be designed and constructed. A physical version will illuminate important aspects of the system that may or may not be included in the modeling and allow further research on the topic. The initial prototype will use less PZT cells than a final actuator and may change gear tooth shape and PZT cell design from the model.

Chapter 4

Dual Sensing and Actuation

4.1 Two-way Electromechanical Transformer

4.1.1 Self-Sensing Actuation

PZT is an electromechanical transformer [5]. Applying a voltage to PZT material will cause the material to strain. Conversely, straining PZT material will induce a voltage across the material. PZT stack actuators are constructed such that a voltage will cause the stack to expand axially. Mechanical compression in the axial direction will induce a voltage across the stack's leads. The two-way transformer nature of PZT allows the stack actuator to act as both an actuator and a sensor. PZT stacks have been used extensively in both applications.

Others have also utilized the PZT actuators simultaneously in both roles [5, 6, 7, 8, 9, 10]. Termed self-sensing actuation, the method monitors the voltage variations superposed on the desired voltage driving signal. The mechanical stimulus on the piezo element causes these voltage variations through the piezoelectric effect. In this way, the PZT stack can provide information about its mechanical loading while simultaneously in use as an actuator. A few general approaches to self-sensing actuation are utilized. One approach first chooses a resistance and capacitance to match the lumped parameters of the piezo. These components and the piezo are used in a number of different bridge circuits to extract the difference between the response of

piezo and the response of the matched components [5, 9, 10]. In other words, the bridge circuits aim to monitor only the voltage variations due to the piezoelectric effect.

However, errors in the choice of capacitance and resistance values or changes in the piezo lumped parameters due to temperature variations or other outside stimulus can cause errors in this technique and lead to instability with feedback. Many of the variations in self-sensing actuation approaches are designed to mitigate these problems. In one case, capacitors are added in series and parallel to decrease the variations in the piezo's capacitance due to temperature variations and thus improve stability of the bridge [7]. Another approach uses a dummy piezo as the matched components in the bridge circuit [10]. In this way, any stimulus which effects the main piezo also effects the dummy piezo in the bridge except the piezoelectric effect experienced by loading the main piezo. Another approach is to use system identification and state estimation to emulate the bridge in software [8]. In software, the parameters or the bridge can be modified to deal with error and changes in the piezo's lumped parameters. Self-sensing actuation has also been used to monitor structure health [6]. This application does not utilize a bridge circuit, but instead monitors the piezo's admittance as the piezo excites the structure. Over time, the change in the piezo's admittance gives information about the health of the structure. All of these approaches use simultaneous actuation and sensing in different fashions. The approach utilized in this work differs greatly and is significantly simpler.

4.1.2 Applicability of Self-Sensing Actuation to Distributed Actuation

Shown in the following sections, self-sensing actuation is overly complicated for the distributed actuation problem as stated in 3.2. However, even if using self-sensing actuation were desirable, the method has many drawbacks when viewed in the context of the problem. The intended design of the actuation and drive system is for high power efficiency, minimization of sensors, and avoidance of complex modeling.

However, different approaches to the self-sensing actuation seem to compromise these desires. Furthermore, the careful design of the flexure system for each cell prevents the use of some classic methods of self-sensing actuation.

First, a bridge circuit utilizing physical inductors and resistors to match the piezo's impedance would require the power source to power the entire bridge circuit. Even without consideration of the additional power for required chips, this method would immediately consume approximately twice the power of simply driving the piezos. This problem is the same when a dummy piezo is used instead of physical components. However, in this problem, this scheme would also require an additional piezo for each one actually used for actuation. The increase in weight, cost, and number of piezo elements is extremely undesirable.

Second, the method of using system identification, modeling, and state estimation to avoid using physical components in the bridge scheme requires a complex model of the system and then often utilizes system identification to populate the parameters of the model. Then, a control scheme is implemented using this model for state estimation with changing parameters to ensure stability. All of these steps are required to monitor the sensing component of the piezo's voltage. With a system objective in this application to minimize or eliminate the need for complex modeling, this method would be highly undesirable.

Finally, the design of the flexure system itself prevents these piezo stack actuators from being used for self-sensing actuation as in [5]. However, the flexure design also prevents the piezo stacks from being misused. Piezo stacks are not meant to be loaded in tension. Tension can cause delamination of the layers and damage to the piezo. The piezo stack in [5] is directly connected to the mass in the system. For certain applications, this method may prove acceptable, but in many situations this direct connection with no antagonistic actuator or spring force could allow the stack to be brought into tension.

The flexures are designed in two layers. The piezo's have an interference fit in the first layer. As the piezo stack expands, the output of the first layer contracts. In response to this contraction, the second layer also contracts. The design was imple-

mented to avoid compression of the flexures which may lead to buckling. All flexure components are in tension. However, this design also prevents the piezo stacks from being loaded incorrectly. If at any time the first layers connection with the piezo stacks themselves expanded, the stacks would simply fall out of the flexures. This design prevents the incorrect loading of the stacks. However, the design also guarantees that the PZT cell can only pull on an external load. Thus, some antagonistic force, whether from gravity, a spring, or another actuator, must exist if the load hopes to guarantee a full return stroke or oscillation. The design prevents the cells from being used in the above mentioned self-sensing actuation scheme because the cells cannot sense forces exerted in both directions. The only way to avoid this problem is to sufficiently pre-load the flexures such that the required negative voltages will arise without the stacks falling out of the flexures. Care would be necessary to ensure this pre-load was properly designed and implemented, and the pre-load may decrease the performance of some aspects of the actuator.

However, regardless of the drawbacks associated with self-sensing and actuation for this application, the method is simply too complicated for the desired application. The system can be designed such that inactive cells can be used as sensors. The following sections discuss this method and its validity.

4.2 System Utilizing Dual Sensing and Actuation

A simple pendulum system was built to demonstrate the use of the proposed driving circuitry and dual sensing and actuation on a system actuated by a distributed set of the developed PZT cells. 4-1 shows a graphical representation of the pendulum system. Lever arms rigidly connect the PZT cells to a mass hung at the bottom. The pendulum rotates at the pivot shown. The PZT cells provide the force to the upper lever arms to cause the pendulum to swing.

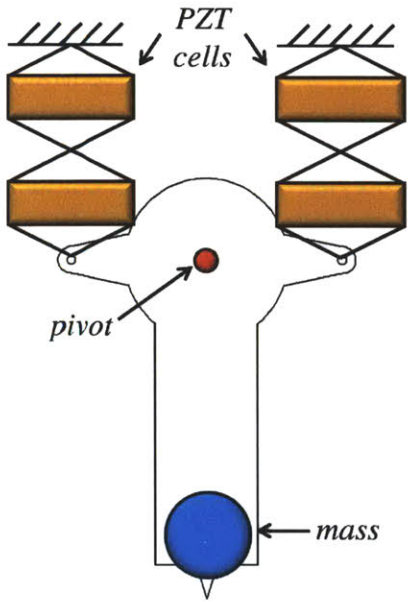

Figure 4-1: Pendulum system actuated by two banks of PZT cells.

4.3 Charge Recovery Circuit

Discussed in 3.4, the charge recovery circuit utilizes two banks of PZT cells which require actuation 180° out of phase to increase the power efficiency of the system. Instead of driving the cells to full voltage and back to ground individually, the circuit utilizes an inductor to move the charge from one set of cells to the other thus supplying much of the energy needed to charge the discharged set while simultaneously sinking much of the energy that must be removed from the charged set. This scheme has many applications when these sets are antagonistic pairs on a load as well as other applications.

4.4 Dual Sensing and Actuation

Because of this charging scheme, one set of PZT cells in each of these pairs is unused while the other is active. In this way, these inactive cells can be used as a sensor in the system. While many applications can utilize this inactive cell as a sensor, perhaps the clearest use is once again when the PZT cell sets are used in antagonistic pairs

on the load as in the test system shown in 4-1.

As stated above, each set of cells can only contract to provide force to the system. While the active set contracts, the systems motion causes extension of the passive set. This cell expansion compresses the PZT stacks inducing a voltage across their leads. This voltage will relate to the magnitude of the expansion. Unlike self-sensing and actuation, this simpler scheme utilizes both the sensing and actuation capability of PZT interchangeably rather than simultaneously. No carefully tuned bridge circuitry or careful separation of signals is necessary to sense in these applications.

One important parasitic which arises in the system is similar to the capacitor self-recharging phenomena. During a very short period of time, the cell is driven from full voltage to zero and then allowed to float. Because insufficient time elapses while the PZT cell is shorted, some amount of charge builds up again on the PZT stacks. Although only a few volts, this voltage make sensing with the cell very difficult. To solve the problem, a resistor is placed in parallel with the stack. An appropriate value is chosen such that the PZT capacitance drains any remaining energy sufficiently fast such that the stacks can reliably sense the mechanically-induced voltage. To avoid energy losses during charging, this parallel resistor is only connected across the PZT cell during the periods of sensing by utilizing an additional MOSFET.

4.5 System Identification

In this sensing and actuation scheme, the inactive PZT cells provide information of the size of the oscillation during the half period of inactivity. Thus, utilizing the information from both sets during their inactive periods, information about the entire oscillation can be recovered. The amplitude of the two halves of the sensor signal for one period gives a direct indication of the amplitude of the oscillation for that period. Although classic frequency sweeps utilize sine waves, this system can only be driven with square waves. However, in the same way, the system can be driven with different frequency square waves while the amplitude of the sensor signal at each frequency is monitored. The magnitude of the input to sensor signal relationship can then be

determined. A type of bode plot can be generated from the square wave input signal to the PZT cell sensor signal.

4.6 Resonance

One important use of this type of system identification is to find the resonance of the system. Many applications can utilize a mechanical resonance in the displacement amplitude. For example, locomotion may use resonance to achieve maximum speed or another desirable outcome. Additionally, applications utilizing PZT often suffer from limited stroke. Therefore, in these applications, a mechanical resonance may be very useful.

Utilizing the system identification method above, the resonance of the input signal to sensor signal relationship can be found. This can be done online very simply by monitoring the sensor signal at each frequency and determining the frequency in which the signal oscillation has the largest amplitude. However, the relationship between the sensor signal amplitude and the mechanical amplitude of the system is not intuitively obvious for a PZT cell attached to a load. Unless the resonance of the desired amplitude coincides with the resonance of the sensor signal or can be deterministically related, the sensor signal cannot be used to determine the systems resonance. Fortunately, the poles of the input signal to sensor signal system are identical to the poles of the input signal to load amplitude system. This results makes intuitive sense because with multi-input-multi-output systems, the loop transfer remains the same for any choice of input and output which would lead to the same poles for both transfer functions.

4.7 System Model

A simple example can show this result. Again, consider the swinging pendulum system shown in 4-1. This system can be modeled as shown in 4-2. Similar to the model of the PZT cell and gear discussed in 3.8, simplifications are made for ease of

modeling. Again, the model will only involve lumped parameters. Second, although each side of the pendulum is actuated by two PZT cells, the model considers a pair of single PZT cells actuating the pendulum. The use of two PZT cells in the real system only increases the maximum amplitude of the pendulum swing and changes certain parameter values, but as an approximation, does not affect the model form itself. Third, the system moves through multiple states. At one point in time, one set of cells is an actuator while the other is a sensor. At another point in time, both sets are coupled electrically through the drive circuitry. Then, the cells switch roles as sensor and actuator. This model simply analyzes the moment when one cell is used to actuate the system while the other cell is used as a sensor.

As shown in 4-2, the model breaks the system into three parts: the rotational system, the actuating PZT cell, and the sensing PZT cell. The rotational system consists of a lumped mass m rotating at a distance b from the pivot. The PZT cells are attached to the system through lever arms of length a. The chosen values for the physical implementation of the system lead to a final assumption of small angles used in the modeling and analysis. a is 25.4 [mm] while the displacement of each PZT cell is on the order of 1 [mm]. Assuming a total stroke of 2 [mm] for the stacked cells, the angle change would be

$$\tan^{-1}(\frac{2}{25.4}) \approx 0.07857\ [rad]$$

Comparing the sine of this angle to the angle itself will indicate the validity of the small angle approximation. The sine of this angle is 0.07852 which is extremely close to the angle itself. Thus, the small angle approximation is appropriate for this system implementation.

The actuating PZT cell and sensing PZT cell models are nearly identical and very similar to the model described in 3.8. The two models only differ in the electrical domain by one component. The actuating PZT then has a voltage source in parallel with both the PZT capacitance and dependent current source. The voltage source drives the system. The sensing PZT instead has an additional impedance in parallel

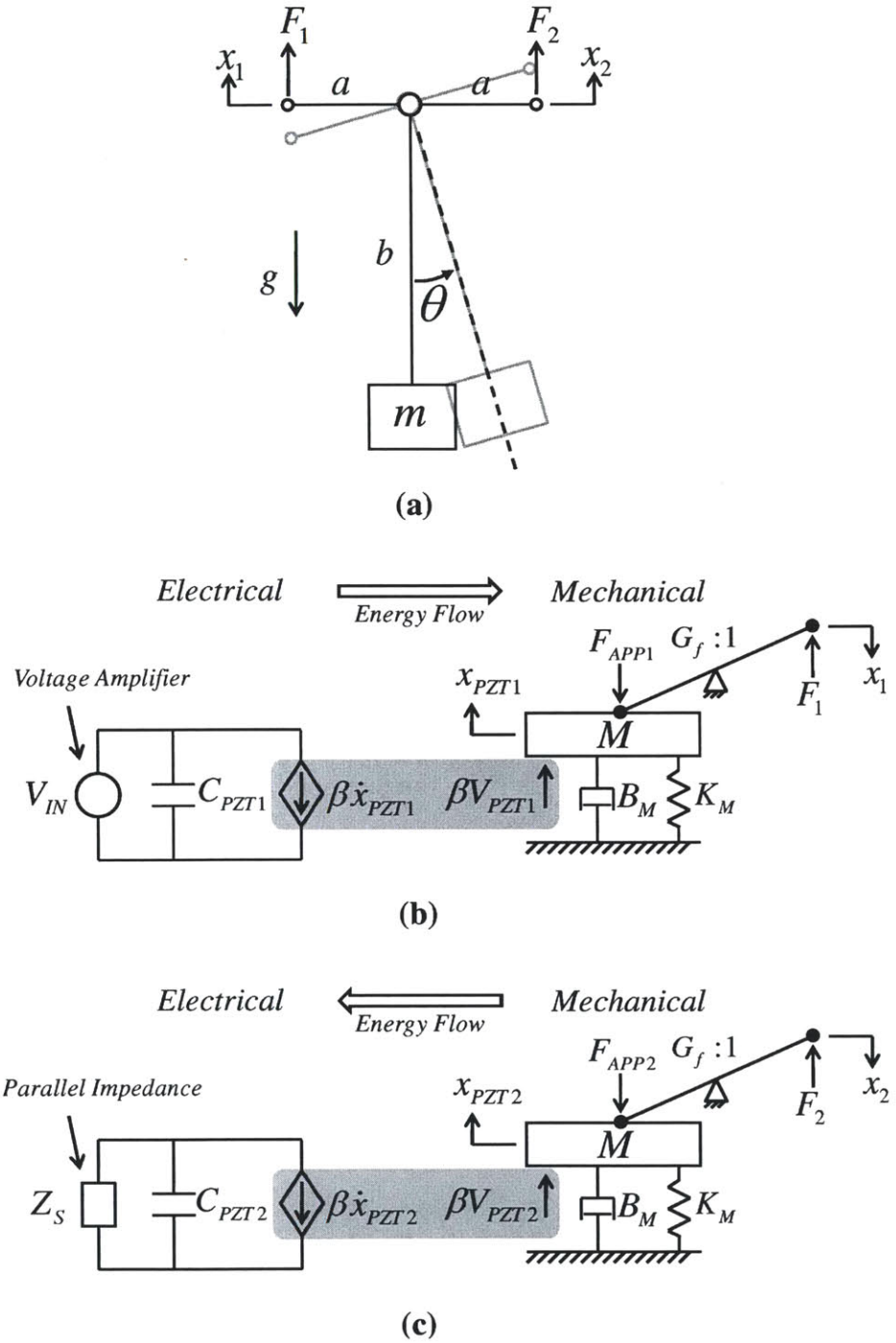

Figure 4-2: Lumped-parameter system model of (a) the rotational system, (b) the actuating PZT cell, and (c) the sensing PZT cell.

with these elements. The parallel impedance represents the sensing impedance and also the draining resistor discussed in 4.4. Shown in 4-3, in this implementation the sensing impedance is dominated by a voltage divider circuit utilizing two resistors to scale the PZT drive voltages that are between 100 and 150 [V] to a level which can be read by standard data acquisition hardware.

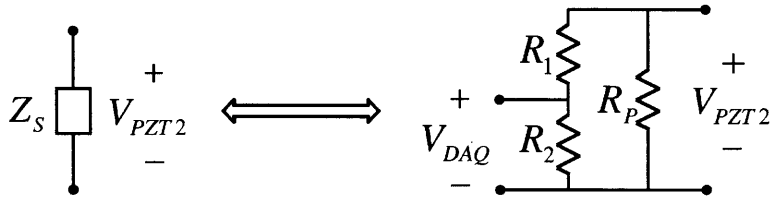

Figure 4-3: The parallel impedance is dominated by the draining resistor and the sense impedance which is dominated by the voltage divider circuit.

With this model, the governing equations of the system were developed. The goal of this analysis is to show that for the same frequency of input voltage, the resonance in the sensed voltage occurs at the same frequency as the resonance in the pendulum displacement. Two transfer functions must be compared. One transfer function is between the input voltage V_{IN} and the output pendulum displacement θ. The other is between the input voltage V_{IN} and the output sensed voltage V_{PZT2}. The following derivation shows that both of these transfer functions share the same poles and thus have the same resonant frequency.

The governing equations for each part of the system can be derived first and later combined to find the transfer functions. For the rotational system the equation of motion is

$$-mgb\theta + a(F_2 - F_1) = mb^2\ddot{\theta}$$

After using the proper reflected quantities, the governing equations for the two PZT cells are

$$\beta V_{PZT1} - B_M\dot{x}_{PZT1} - K_M x_{PZT1} - G_f F_1 = M\ddot{x}_{PZT1}$$

$$\beta V_{PZT2} - B_M\dot{x}_{PZT2} - K_M x_{PZT2} - G_f F_2 = M\ddot{x}_{PZT2}$$

Combining the equations is easiest in the frequency domain. After substitution and rearrangement, the laplace representations of the above equations are

$$a(F_2(s) - F_1(s)) = (mb^2s^2 + mgb)\theta(s)$$

$$\beta V_{IN}(s) - G_f F_1(s) = (Ms^2 + B_M s + K_M)X_{PZT1}(s)$$

$$\beta V_{PZT2}(s) - G_f F_2(s) = (Ms^2 + B_M s + K_M)X_{PZT2}(s)$$

After rearranging these equations and adding other relations that follow from the model, the following equation emerges giving insight to the applicability of this analysis:

$$(M_i s^2 + B_i s + K_i)\theta(s) = \beta\frac{a}{G_f}(V_{PZT2}(s) - V_{IN}(s))$$

where

$$M_i = \frac{2a^2}{G_f^2}M_m + mb^2$$

$$B_i = \frac{2a^2}{G_f^2}B_m$$

$$K_i = \frac{2a^2}{G_f^2}K_m + mgb$$

This equation suggests that this analysis is applicable to a general load with an equivalent inertia, damping, and stiffness. The forcing term applied to the load is proportional to the difference between the sense voltage and the drive voltage. This generality is important to this analysis's applicability to more general systems and in turn the applicability of the entire dual sensing and actuation method.

The electrical domain of the sensing PZT cell yields the following relationship between V_{PZT2} and θ:

$$\frac{V_{PZT2}(s)}{\theta(s)} = -\beta\frac{a}{G_f}\frac{Z(s)s}{(1 + C_{PZT2}Z(s)s)}$$

Using this relationship along with the previous equations, both required transfer functions can be derived. The two transfer functions are

$$\frac{\Theta(s)}{V_{IN}(s)} = -\beta\frac{a}{G_f}\frac{(1 + C_{PZT2}Z_s(s)s)}{As^3 + Bs^2 + Cs + D}$$

$$\frac{V_{PZT2}(s)}{V_{IN}(s)} = \beta^2\frac{a^2}{G_f^2}\frac{Z_s(s)s}{As^3 + Bs^2 + Cs + D}$$

where

$$A = C_{PZT2}Z_s(s)M_i$$

$$B = M_i + C_{PZT2}Z_s(s)B_i$$

$$C = B_i + C_{PZT2}Z_s(s)K_i + \beta^2\frac{a^2}{G_f^2}Z_s(s)$$

$$D = K_i$$

where M_i, B_i, and K_i are defined above.

The denominators and thus the poles of the two transfer functions are identical. Therefore, the resonance frequency of both transfer functions are identical. This result shows that finding the driving frequency which causes a resonance in the sensed voltage will also indicate the resonance in the mechanical amplitude of the pendulum swing.

4.8 Test Setup

A physical version of the modeled system was developed. 4-4 shows a front view of the system. The mass, pivot, and PZT cells are shown. The two PZT cells on each side of the pendulum are connected mechanically in series but driven in parallel electrically. Thus, each set of cells on one side of the pendulum should be considered a cell bank.

A potentiometer was added to the pivot in the system to measure the angular displacement of the pendulum for verification purposes. 4-5 shows a view of the

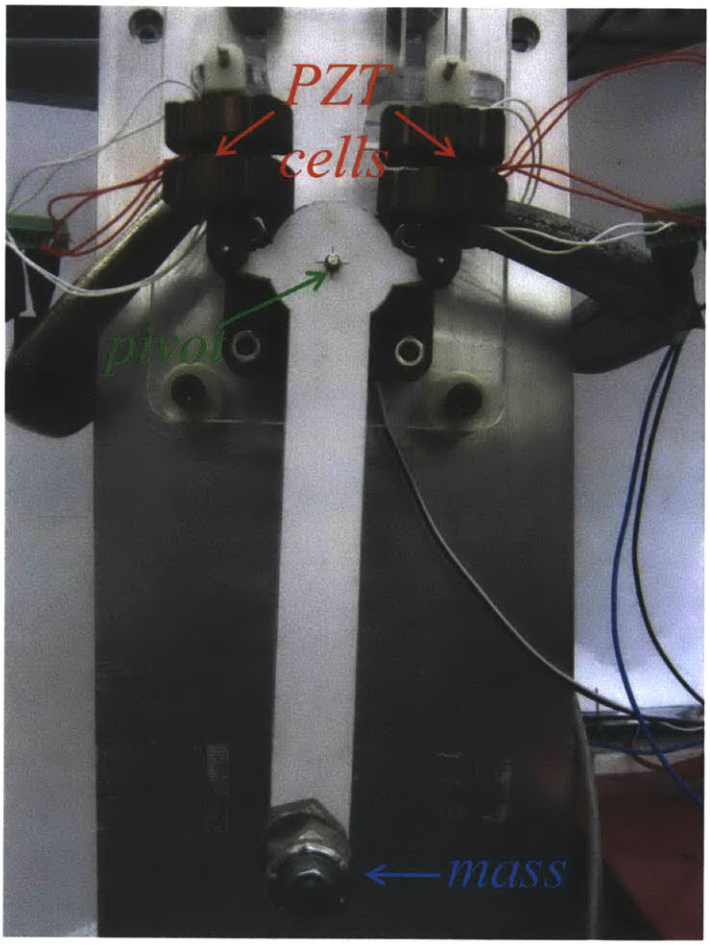

Figure 4-4: Front view of the PZT driven pendulum setup.

system from above to indicate the position of the potentiometer in the system.

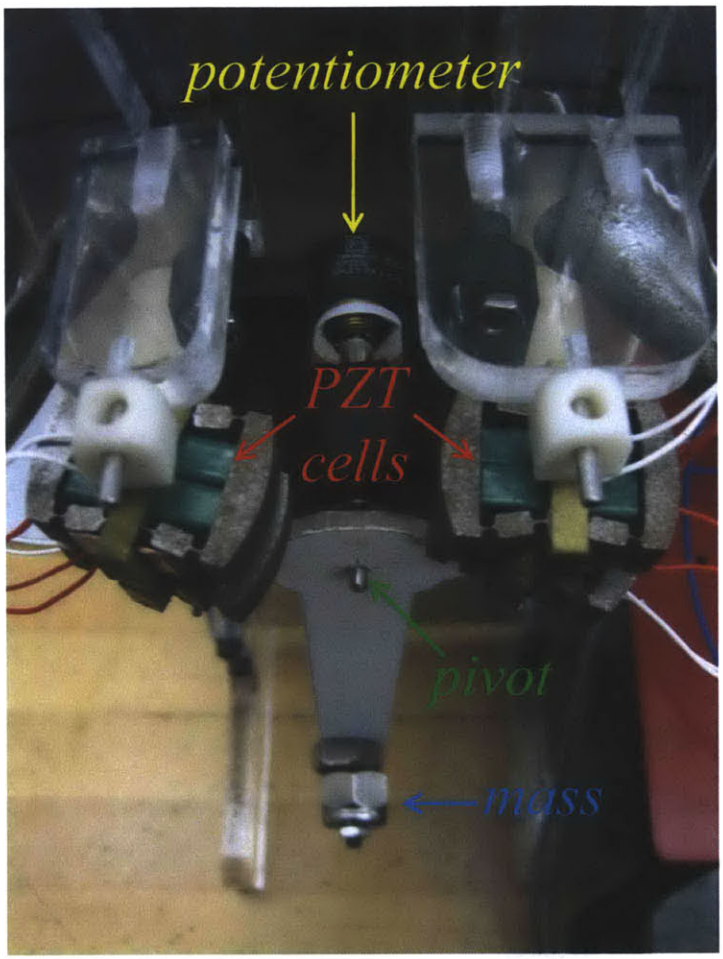

Figure 4-5: Top view of the PZT driven pendulum setup.

The cell banks are connected to the charge recovery circuit described above. A controller drives the this circuit appropriately to produce a square-wave frequency sweep of forces on the pendulum. The controller also monitors and records the sensing voltages from the PZT cells as well as the signal from the potentiometer.

4.9 Simple Algorithm

Using dual actuation and sensing, a system can search for its own resonance frequency online without a model. This online system identification could avoid the use of po-

tentially complex system models or allow for updated resonance frequencies if system parameters change in real time.

One simple method of obtaining the resonance frequency of the system is driving the system with the actuators at different frequencies and monitoring the PZT sensor voltages until finding a frequency which causes the highest amplitude in the sense signals. Then, the system could return to this resonance frequency for operation. Other more complex methods may utilize a controller to continually drive the system to its resonance frequency while the frequency potentially varies in time. However, the experiments examined here use the simple frequency sweep method.

4.10 Results

4-6 shows the normalized voltages from the PZT cell banks and the potentiometer during an impulsive finger flick. This quick experiment shows that the the PZT voltages utilized together accurately trace the potentiometer especially in terms of frequency. The voltage from cell bank 2 is inverted as it corresponds to the negative side of the pendulum motion. The amplitude of the signals can vary based upon many factors in the mechanical system and electrical circuit. Thus, some calibration would be necessary to ensure the PZT sense voltages had physical meaning if that functionality was necessary. The normalized voltages in 4-6 show that with this type of calibration the PZT sense voltages could also accurately represent the magnitude of the physical oscillation.

The input actuation frequency was swept between 0.5 [Hz] and 9.5 [Hz] (3.14 $[\frac{rad}{s}]$ and 59.69 $[\frac{rad}{s}]$) while the PZT sense voltages and potentiometer voltage were recorded over time. 4-7 shows the results of this experiment and indicates that the PZT sense voltages closely trace the potentiometer voltage during the frequency sweep. Visual inspection suggests that the resonance peak occurs at approximately the same frequency for all of the signals. This match was expected from the model analysis outlined above. Some jittering occurs in the signals during the sweep. All of the signals seem to experience the same problem which appears to come from some in-

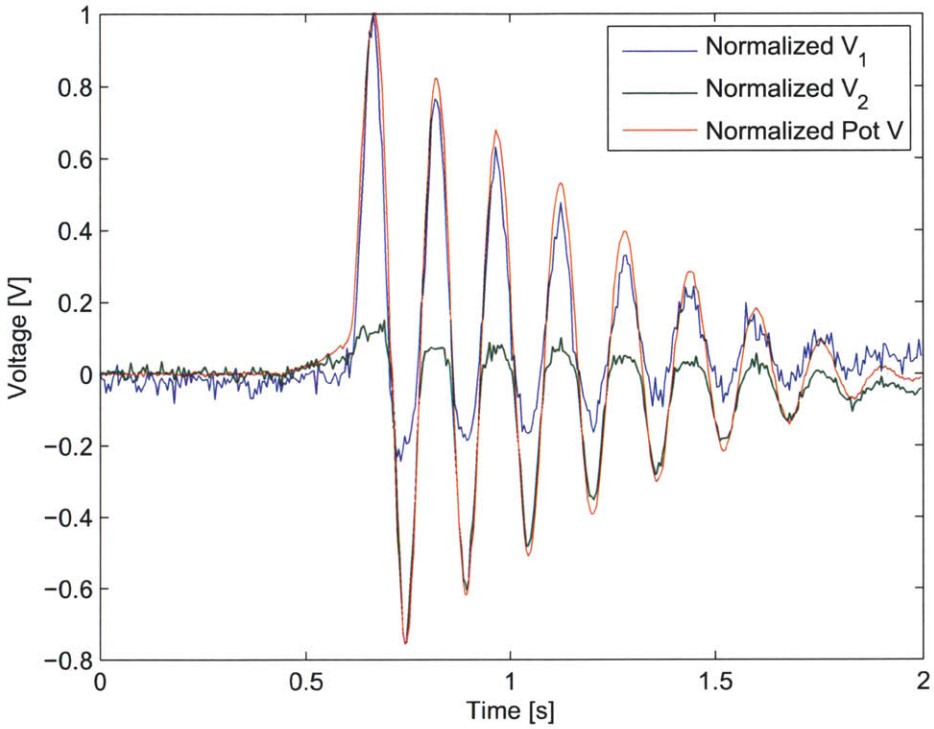

Figure 4-6: Response to finger flick measured by potentiometer and both inactive PZT banks.

consistency in the controller driving the system. This jitter does not substantially affect the conclusion of the experiment that indeed the PZT sense voltages correctly trace the potentiometer voltage over this range of frequencies.

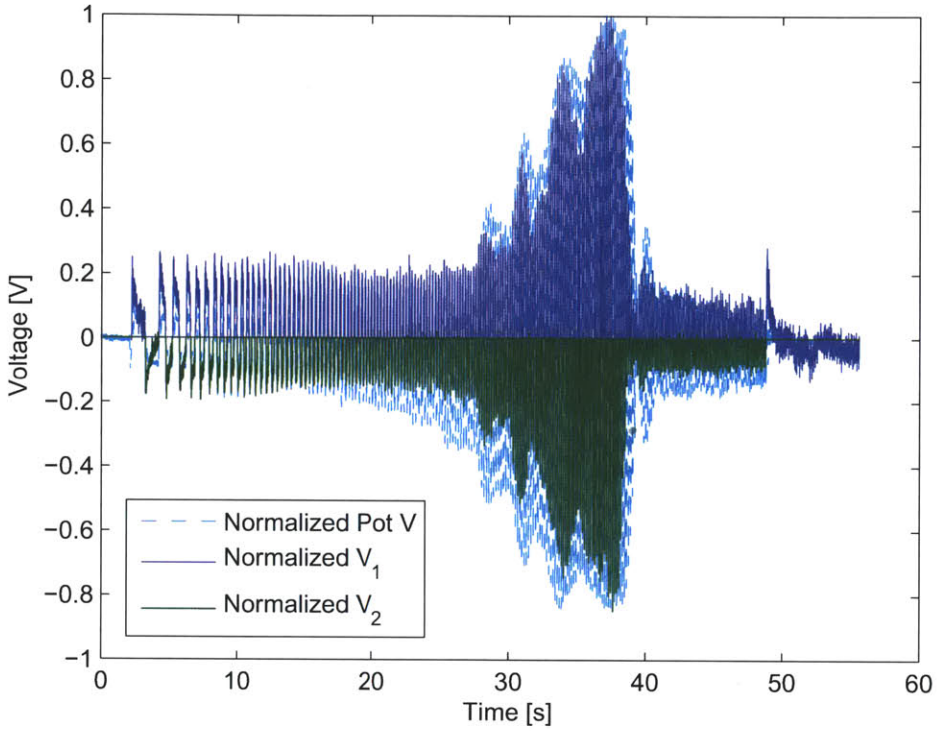

Figure 4-7: Pendulum displacement to a swept frequency input over time measured by potentiometer and inactive PZT bank.

The potentiometer voltage measures the entire range of θ while each of the PZT cell banks only measures one direction of the swing. For comparison, the potentiometer voltage was then split into a positive signal and negative signal. These two signals and the PZT sense voltages were used to generate bode magnitude plots to compare the resonant frequency predicted by the different signals. 4-8 shows the normalized magnitudes versus frequency of the four signals. Each signal individually predicts that the natural frequency occurs at 7.5 [Hz] (47.1 $[\frac{rad}{s}]$). The resolution of the frequency sweep is relatively low at using 0.5 [Hz] (3.14 $[\frac{rad}{s}]$) steps, and thus this result does not confirm that each signal will always predict the exact same resonant frequency.

However, the data suggests that the signals will show close agreement and that with only the PZT cell banks as sensors, the system can still accurately find its resonance frequency within at least approximately ± 7%.

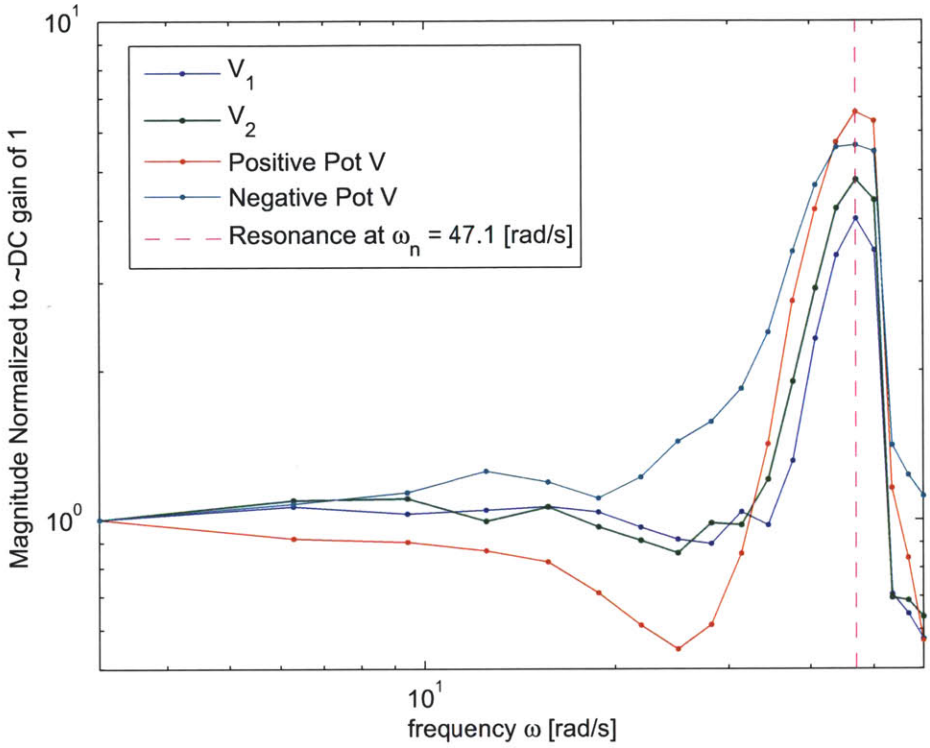

Figure 4-8: Normalized magnitudes versus frequency for PZT sense voltages and potentiometer voltage.

Chapter 5

Conclusion

The PZT cellular actuator provides many possibilities through the use of charge recovery, distributed actuation, and dual sensing and actuation. Initial exploration into active drive circuitry revealed the impracticality of energy harvesting at the scale used, unwanted design and control complexity, and other problems. The functional requirements of the circuit were reevaluated with careful consideration of the desire to distribute many actuators on the same load.

With PZT cells distributed on a mechanical load, many functionalities can be achieved. First, a method of efficient distributed actuation on a mechanical system with PZT cells was proposed. PZT cells would be grouped in banks which would transfer energy between different banks in a controlled fashion to produce the desired system motion. Second, a charge recovery circuit was designed and implemented to achieve this charge transfer. Without optimization, the circuit successfully transfers 65% of the voltage from the activated to deactivated PZT cell which equates to ~41% energy savings compared to not using charge recovery. This energy savings makes the proposed distributed activation method very energy efficient compared to standard drive methods. Next, distributed actuation was applied in simulation to a linear gear where multiple PZTs drive the gear in parallel. The model incorporated the dynamics of both the gear system and the PZT cell. With the conditions chosen for this simulation, the idealized no-load, steady-state velocity of the gear was 2.4 $[\frac{m}{s}]$.

Finally, the electromechanical transformation properties of PZT were used to de-

velop a dual sensing and actuation method using distributed PZT cells. With this functionality, the active cell still actuates the system. However, now the inactive cell is used to sense the amplitude of the motion. In this way, using no external sensors, the system can identify its own resonance. These functionalities and their possible extensions and uses show the importance and impact that charge recovery, distributed actuation, and dual sensing and actuation with the PZT cellular actuator can have on robotic systems.

Bibliography

[1] M. Bergamasco, F. Salsedo, and P. Dario, "A linear sma motor as direct-drive robotic actuator," in *IEEE international conference on Robotics and Automation*, pp. 618–623, IEEE, 1989.

[2] T. Secord and H. Asada, "A variable stiffness pzt cellular actuator with tunable resonance for cyclic motion tasks," in *IEEE international conference on Robotics and Automation*, pp. 176–181, IEEE, 2009.

[3] D. Campolo, M. Sitti, and R. Fearing, "Efficient charge recovery method for driving piezoelectric actuators with quasi-square waves," *IEEE transactions on ultrasonics, ferroelectrics, and frequency control*, vol. 50, no. 3, pp. 237–244, 2003.

[4] M. Karpelson, G. Wei, and R. Wood, "Milligram-scale high-voltage power electronics for piezoelectric microrobots," in *IEEE international conference on Robotics and Automation*, pp. 2217–2224, 2009.

[5] L. Jones, E. Garcia, and H. Waites, "Self-sensing control as applied to a pzt stack actuator used as a micropositioner," *Smart Materials and Structures*, vol. 3, pp. 147–156, 1994.

[6] F. Sun, Z. Chaudhry, C. Liang, and C. Rogers, "Truss structure integrity identification using pzt sensor-actuator," *Journal of Intelligent Material Systems and Structures*, vol. 6, no. 1, pp. 134–139, 1995.

[7] G. Simmers Jr, J. Hodgkins, D. Mascarenas, G. Park, and H. Sohn, "Improved piezoelectric self-sensing actuation," *Journal of Intelligent Material Systems and Structures*, vol. 15, no. 12, pp. 941–953, 2004.

[8] M. Okugawa and M. Sasaki, "System identification and controller design of a self-sensing piezoelectric cantilever structure," *Journal of Intelligent Material Systems and Structures*, vol. 13, no. 4, pp. 241–252, 2002.

[9] Y. Miyahara, M. Deschler, T. Fujii, S. Watanabe, and H. Bleuler, "Non-contact atomic force microscope with a pzt cantilever used for deflection sensing, direct oscillation and feedback actuation," *Applied Surface Science*, vol. 188, no. 3-4, pp. 450–455, 2002.

[10] C. Lee, T. Itoh, and T. Suga, "Self-excited piezoelectric pzt microcantilevers for dynamic sfm–with inherent sensing and actuating capabilities," *Sensors and Actuators A: Physical*, vol. 72, no. 2, pp. 179–188, 1999.